Limits of Long Wavelength High Harmonic Generation

by

Siddharth Bhardwaj

B.S., Electrical Engineering, Physics (Minor) (2007)

University of Southern California

Submitted to the Department of Electrical Engineering and Computer Science

in partial fulfillment of the requirements for the degree of

Master of Science in Electrical Engineering and Computer Science

at the

MASSACHUSETTS INSTITUTE OF TECHNOLOGY

February 2010

Author..... .....

Department of Electrical Engineering and Computer Science

January 28, 2010

Certified by..... .....

Franz X. Kärtner

Professor of Electrical Engineering

Thesis Supervisor

Accepted by ....

Terry P. Orlando

Chairman, Department Committee on Graduate Students

Limits of Long Wavelength High Harmonic Generation

by

SIDDHARTH BHARDWAJ

Submitted to the Department of Electrical Engineering and Computer Science
on February 1, 2010 in partial fulfillment of the
requirements for the degree of Master of Science in
Electrical Engineering and Computer Science

Abstract

Many researchers are pushing for long wavelength driver pulses for High Harmonic Generation (HHG). The advantage of longer wavelengths is that the cut-off of the harmonic spectrum can be increased without the need for large electric fields. Large electric field is undesirable because it leads to large plasma generation which reduces harmonic generation due to phase mismatch and ground state depletion.

Most of the current literature on HHG uses the Dipole Approximation for calculation of harmonic spectrum. The physical ramification of the Dipole Approximation is that it neglects the magnetic field component to the driver field. It is well known that a charge moving in a magnetic field experiences a Lorentz force. In HHG, harmonics are generated by recombination of an electron wave packet, moving under the influence of the driver pulse, with its parent atom. The Lorentz force can displace the electron wave packet perpendicular to the direction of polarization and as a result reducing the recombination amplitude. This Lorentz displacement increases as we move towards longer wavelengths and higher intensities. In this thesis, intensity and wavelength limits at which the Lorentz displacement becomes significant have been investigated.

By numerically solving the time-dependent Schrödinger equation, we investigate the optimum driver pulse duration for 400 nm, 800 nm and 2 micron driver pulses for a given harmonic for hydrogen. It was found that longer wavelength have smaller efficiencies (neglecting phase matching condition).

Finally, the harmonic spectrum of Hydrogen driven by 800 nm pulse predicted by analytic Three Step Model (TSM) has been compared with the harmonic spectrum generated by numerical solution of time-dependent Schrödinger equation. It was found, as the current theories predict, that TSM becomes less reliable as the Keldysh Parameter increases. It was also observed that for low harmonic energies,

the TSM spectrum deviates from the numerical spectrum by many orders of magnitude.

Thesis Supervisor: Franz X. Kärtner

Title: Professor of Electrical Engineering

Εν οίδα ότι ουδέν οίδα

- Socrates

ACKNOWLEDGEMENTS

The last two years at MIT have been pretty challenging and in retrospect I would not have been able to write this thesis without the help and support of friends, colleagues and family. I would first like to thank my group members, particularly Anatoly Khilo, Vasileios Gkortsas and Shu-Wei Huang for many insightful discussions. Anatoly has been an enthusiastic mentor and has spent many hours patiently helping me. I also thank my advisor Franz Kaertner, for his guidance and patience during times when I felt that graduate school was not my cup of tea. Lastly, I am extremely grateful to my family. Without their unwavering support and sacrifice I would have never made it to MIT.

Support

This work was supported by **AFOSR** grant **FA 9550-08-1-0409**

CONTENTS

1. Introduction to High harmonic generation

1.1. Introduction:

Ever since the invention of lasers, scientists around the world have strived to produce short pulses in order to attain high peak power and better time resolution. The development in the field of ultra-fast optics can be observed in Figure 1. Initially, laser pulses were several microseconds in duration. Invention of Q-switching (Hellwarth, 1961) brought the pulse duration down to the nanosecond regime. The field of Ultra-fast optics was set into motion with the invention of laser mode locking in 1964 by Hargrove *et al.* The first generation of mode locked lasers, which produced pulses of durations less than 100 p.s., used solid-state laser materials such as ruby, Nd:glass or Nd:YAG as gain media [1]. The second generation of mode locked lasers, which used broad gain media and saturable absorbers (Ippen *et al.* 1972), lowered the pulse duration down to 1 p.s. Further development in ring cavities and GVD compensation techniques brought the pulse duration down to 6 f.s [2]. These trends can be seen in Figure 1. We see the flattening of the curve during the eighties when the pulse duration did not reduce dramatically. It became apparent in early nineties that a fundamentally different approach was required to produce sub femto-second pulses.

In the early nineties, the theory of High Harmonic generation was developed by atomic physicists who realized that it was possible to produce a broad spectrum of odd harmonics, by placing an atom in a strong laser field. This idea paved the way for the development of attosecond pulses. It took laser physicists about 10 years to actually demonstrate an attosecond pulse. Paul Corkum (who gave Hermann Anton Haus lecture in 2009) in a letter to Nature in February, 2000 remarked; "For the past five years, scientists have stood on the threshold of generating attosecond laser pulses but have been unable to cross it....This may have changed with [measurement of] trains of attosecond pulses" Indeed, since then, pulses of duration ~100 attoseconds have been regularly produced and measured. In this section we will discuss the theory of High Harmonic generation, both semi-classically and quantum mechanically.

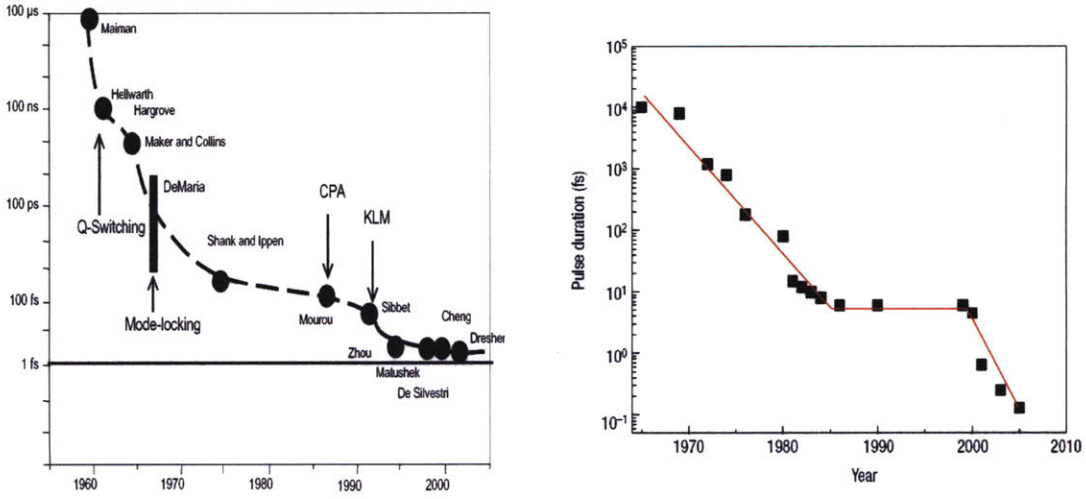

Figure 1. Above figures show the timeline of evolution of laser pulse duration. The left one highlights the important milestones that led to the shortening of pulse as discussed in the introduction. The Right one elucidates the sharp decrease in pulse duration with the advent of HHG theory in 1990's. The left and the right figures have been taken from [2] and [3] respectively

1.2. Semi-Classical description of high harmonic generation:

In spite of being a highly non-linear and a quantum mechanical process, much insight can be gained into High Harmonic Generation by simply analyzing it as a semi-classical process. When a sinusoidal field is shone on an atom, an electron from its outermost orbital is released into the continuum. It is then accelerated by the laser field and when the direction of the electric field reverses, it comes back and collides with the atom. This is called Single Atom Response (SAE) and can be studied using the Three Step Model (TSM) which, as the name suggests, comprises of three steps:

a) Ionization

b) Acceleration

c) Recombination

This can be better understood by looking at Figure 2. In step (a), the electric field (yellow line) alters the shape of the coulomb potential, allowing the electron to tunnel through the

barrier and emerge in the continuum. In steps (b) and (c) the electron travels classically in the continuum (neglecting the influence of the coulomb potential) and returns back to the atom when the electric field reverses directions. In step (d) the returning electron collides with the atom and may be classically scattered or absorbed inelastically. In case of the latter, its kinetic energy is released as a burst of photon energy. This is the high harmonic pulse (represented by the blue line in (d)). Step (e) is the quantum mechanical description of this process. It should be noted that each of the classical steps can be described quantum mechanically. We will return to the quantum mechanical idea in the next section.

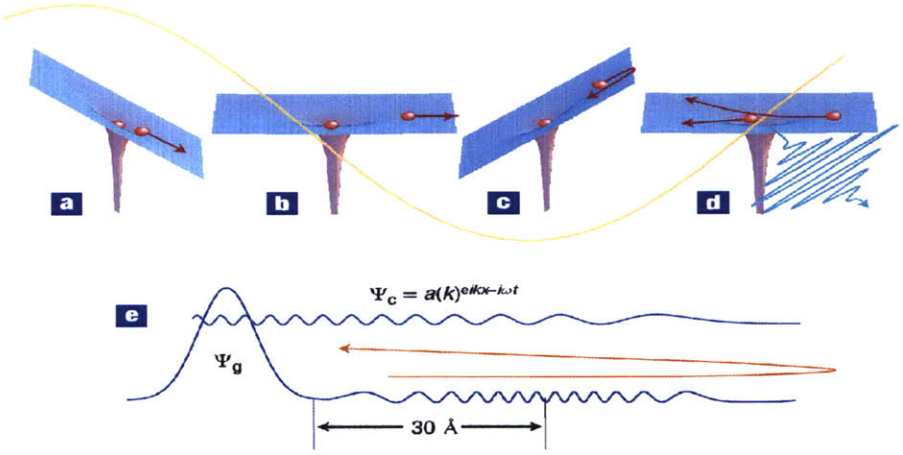

Figure 2: Three step process in HHG. (a),(b),(c),(d) show the classical trajectory of the electron. (e) represents the quantum mechanical wave function of the atom split into the ground state and traveling wave. This plot is taken from [3]

Let us continue with semi-classical analysis: when an electron is placed in an electromagnetic field, it begins to quiver with average Kinetic Energy called ponderomotive energy. It is defined as:

$$U_p = \left(\frac{qE}{2m_e\omega}\right)^2 = \left(\frac{E^2}{4\omega^2}\right) \tag{1.1}$$

As we will see later, the high harmonic spectrum is critically dependent on this factor. Lets us look at each of the three processes in a little more detail:

i) Ionization: For high harmonic generation we only use those driver pulses whose $\omega < I_p$. ω is the frequency of light and I_p is the ionization potential of the atom. Note that $\hbar = 1$ in atomic units. Additionally, electronic charge and mass are also taken to be one. The electron can be ionized for the parent atom by three distinct processes See Figure 3

Multiphoton ionization regime: This takes place when $E << 1au$ (driving electric field is much less than one atomic unit) and $U_p << I_p$. This process is dominant when the driving electric field is weak and the electron absorbs several photons to get ionized. The ionization has a power law dependence on intensity.

Barrier Suppression Regime: In this regime the electric field is so strong that the coulomb barrier is completely suppressed and the electron is free to move into the free space. In this case ionization has linear dependence on incident electric field.

Tunneling regime: In this third and the most important regime for high harmonic generation, the electric field is stronger than in the multi-photon ionization case but not strong enough to completely suppress the barrier like the barrier suppression regime. It is characterized by an exponential dependence of the ionization rate on field intensity [4].

$$w(E) \sim \exp\left(-\frac{2(2I_p)^{3/2}}{3E}\right) \tag{1.2}$$

High harmonic generation utilizes tunneling for releasing an electron wavepacket which will return back to the atom with energy proportional to the ponderomotive energy. Due to tunneling the bounded electron wavefunction decays exponentially:

$$|a(t)|^2 = \exp\left(-\int_0^t w(E(t')dt'\right) \tag{1.3}$$

Where $a(t)$ is the probability amplitude of finding the electron in the ground state. A more in-depth quantum mechanical calculation of tunneling can be done using Ammosov-Delone-Krainov (ADK) formula[5].

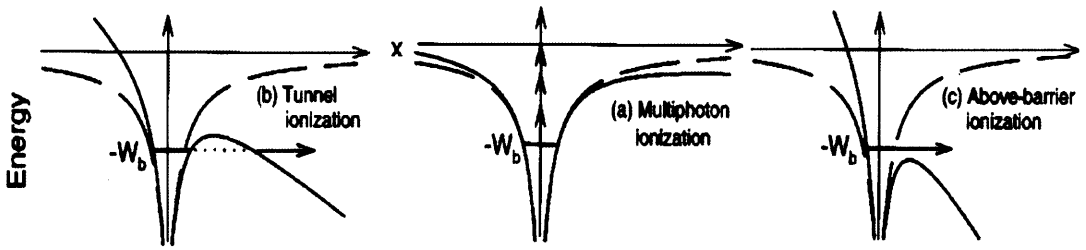

Figure 3: Different ionization regimes. This plot is taken from [1].

ii) Acceleration: It is assumed that when the electron tunnels out of the atom instantaneously and has zero kinetic energy. (In reality this may not be the case and the electron may have some transverse velocity after it tunnels out.) Once it has emerged, it is accelerated by the sinusoidal electric field. Classically, we can write the equation of motion for this electron (again in atomic units)

$$\ddot{x}(t) = E_0 \cos \omega t \tag{1.4}$$

$$\dot{x}(t) = \frac{E_0}{\omega} \sin \omega t - \frac{E_0}{\omega} \sin \omega t_0 \tag{1.5}$$

$$x(t) = -\frac{E_0}{\omega^2} \cos \omega t - (t - t_0)\frac{E_0}{\omega} \sin \omega t_0 + \frac{E_0}{\omega^2} \cos \omega t_0 \tag{1.6}$$

t_0 is the time of birth of the electron. Quantum mechanically there is no fixed time when the electron tunnels out. Rather, there is a range of times when it can tunnel out with a certain probability. The time of birth of the electron with respect to the electric field is critical in determining whether the electron is going to return back to the nucleus or not. As we can see from Figure 4 only those trajectories that touch the horizontal black dotted line hit the parent ion.

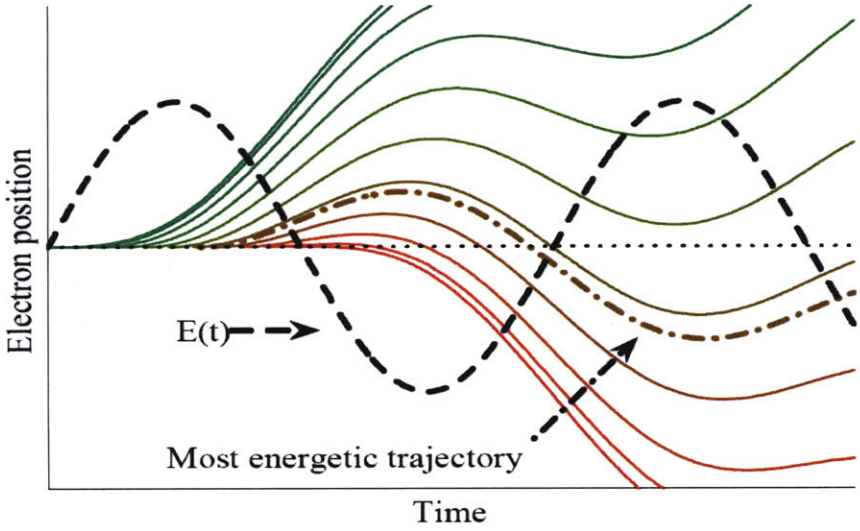

Figure 4: Classical electronic trajectories with respect to the driving pulse (black dashed line). This plot was taken form [6].

We first need to solve for t such that $x(t) = 0$ (for a given t_0). Then plug it in the expression for $\dot{x}$. This gives the kinetic energy at that time instant. It is easy to solve it for a range of birth time t_0 using a computer program. It has been found that only those electrons return back to the parent ions, which have been ionized when the electric field begins to decrease after reaching its maxima. The most energetic trajectory (corresponding to the brown dashed-dotted line in Figure 4) has kinetic energy equal to $3.17U_p$. The ratio of kinetic energy to the ponderomotive potential and their position in the electric field is shown in Figure 5.

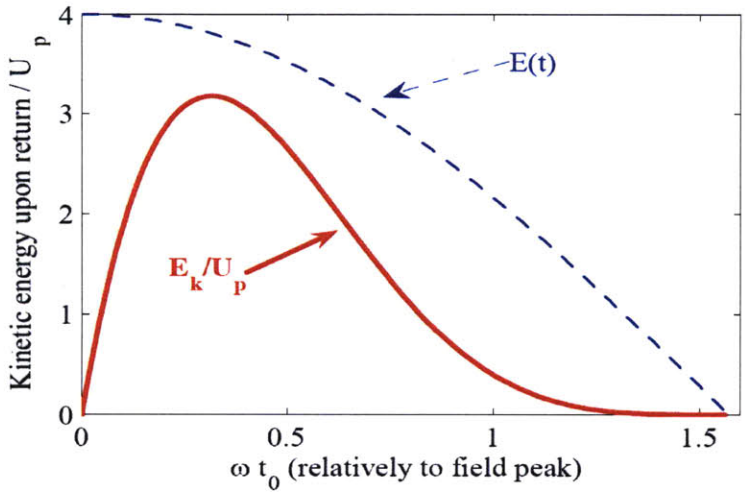

Figure 5: Red line shows the ratio of the kinetic energy and the ponderomotive energy upon the return of the electron to the atom as a function of birth time. This plot was taken from [6][10].

iii) Recombination: Once the electron returns back to the parent ion, it "falls" to the ground state releasing energy in the form of a photon burst. The emitted radiation has a wide spectrum reaching up to about 150 harmonics (150 times the frequency of the driver pulse.) Putting this in perspective, we regularly encounter $\chi^{(2)}$ and $\chi^{(3)}$ processes in Non-Linear Optics (which produce second and third harmonics respectively.) We clearly see the advantage of high harmonic generation for producing extremely high frequencies. The highest frequency produced is called the "cut-off". It is the energy corresponding to the most energetic trajectory in Figure 4. It's given as:

$$\omega_{\max} = I_p + 3.17U_p \tag{1.7}$$

Recombination is a quantum mechanical event, and it has hard to describe it in detail classically. We will come back to it in the next section.

The exact way of describing a quantum mechanical system is to write its Schrödinger equation which tells us how a quantum state propagates in time.

$$i\frac{\partial|\Psi(x,t)\rangle}{\partial t} = \left[-\frac{1}{2}\nabla^2 + V(x) - E\cos(t)x\right]|\Psi(x,t)\rangle \tag{1.8}$$

Unfortunately, it is not easy to solve the above equation analytically even for this simplified case. To solve it people use Numerical Time Dependent Schrödinger Equation (NTDSE). In

spite of providing a solution of the above equation NTDSE does not help us in developing an intuition about HHG process. To do so, we need to come up with an approximate quantum model based on our intuition of the process.

We begin by defining a new term called the Keldysh Parameter

$$\gamma = \sqrt{\frac{I_p}{2U_p}} = \frac{\omega\sqrt{2I_p}}{E} \tag{1.9}$$

When $\gamma << 1$, we are in the tunneling regime or barrier suppression regime. Alternative interpretation of Equation 6 is that when $\gamma << 1$, the time it takes for the electron to tunnel is much smaller than the time period of the driver pulse. For example, for a 800 nm driver pulse (time period about 2.7 femto-seconds), the tunneling takes place in about 300 attoseconds around the field crest of the pulse peak [3]. The electron leaves the atom when the driver pulse is close to its peak. Once it emerges, it is accelerated by the electric field and attains about 50-1000 eV [3] during its first femtosecond of freedom. Due to this large kinetic energy, we can neglect the effect of the atomic potential ($-\nabla V(x)$). Later we shall see that this is called the Strong Field Approximation (SFA). The kinetic energy decreases when the electron slows down after the field reverses direction. But at that moment the electron is far away from the atom and once again the atomic potential can be neglected. This assumption is particularly true for short range potentials. However, it also seems to work pretty well for long range potential like Hydrogen atom. Due to the aforementioned assumptions, the path of the electron can be treated classically. Hence we can say that for each birth time the electron follow a classical trajectory (all governed by the classical equations presented in the last section). The most energetic trajectories which are born at $t_1 \approx \frac{1.88}{\omega_0}$, re-collide at $t_2 \approx \frac{5.97}{\omega_0}$ and are responsible for producing the most energetic photons. Another way to think about the recombination event is as follows: a part of the ground state tunnels out of the coulomb barrier, this wavepacket is accelerated by the electric field, and on returning back to the atom it interferes with the ground state left behind. This interference produces a dipole moment that emits light. Most importantly, the energy and the phase information of the electron is coherently transferred to the burst of photons. Conservation of coherence is critical to the HHG process.

1.3. Mathematical Formulation of Electron-Field Interaction

It is worthwhile to review the intuition we have developed thus far and use it to re-derive a mathematical formulation as shown in [7]. This will help us better understand the approximations (like SFA, Dipole approximation) that are found in the current HHG literature.

HHG is produced due to the interaction of bound electronic wave packet with an external perturbation (in our case it is the laser field). The Schrödinger equation for such an interaction is:

$$i\frac{\partial}{\partial t}|\Psi\rangle = (H_0 + V_L(t))|\Psi\rangle \tag{1.10}$$

Here H_0 is the unperturbed atomic potential and $V_L(t)$ is the external perturbation. The exact solution of this equation is given by

$$|\Psi(t)\rangle = -i\int_0^t dt' \left[e^{-i\int_{t'}^{t} H(t'')dt''}\right] V_L(t') \left[e^{-i\int_0^{t'} H_0(t'')dt''}\right] |\phi_i\rangle + e^{-i\int_0^t H_0(t'')dt''}|\phi_i\rangle \tag{1.11}$$

$|\phi_i\rangle$ is the initial bound state. The first term is the particular solution and second is the homogenous solution. The particular solution, although mathematically daunting, has a physical meaning: the bound state evolves until t' under the influence of atomic potential (a simple phase multiplication,) gets a "kick" from the laser field $(V_L(t'))$ and then evolves under the influence of the total Hamiltonian (atomic potential + laser field.) Since, the interaction happens at all times we need to integrate from zero to t. This idea is similar to Feynman Path diagrams which state that a system can go from one state to another by following infinitely many paths.

Now we employ the Strong Field Approximation which is valid for strong low frequency field

i) The electron is instantaneously born into the continuum at time t'

ii) After birth, the electron travels like a plane wave under the influence of electric field only- Volkov Propagator. Mathematically it means

$$H(t) \rightarrow H_V(t) \equiv H(t) - V_A \tag{1.12}$$

iii) Electron is born with zero velocity

For generalization assume that electron is born with velocity v' at time t' and is then accelerated to velocity v at time t. These quantities are related by:

$$\mathbf{v} = \mathbf{v}' - \mathbf{A}(t) + \mathbf{A}(t') \tag{1.13}$$

$A(t)$ is the vector potential of the electric field. One may note that we have inconspicuously introduced the *Dipole Approximation* here by making the vector potential only a function of time and neglecting the spatial dependence. We will talk in detail about this approximation and its implications in Chapter 4.

Projecting Equation 1.11 the velocity/ momentum state $\langle \mathbf{v}|$ we get

$$\Psi(\mathbf{v},t) = -i\int_0^t dt' \langle \mathbf{v}| \left[e^{-i\int_{t'}^{t} H(t'')dt''} \right] V_L(t') \left[e^{-i\int_0^{t'} H_0(t'')dt''} \right] |\phi_i\rangle \tag{1.14}$$

Replacing $H(t)$ by $H_V(t)$,we can write

$$e^{-i\int_{t'}^{t} H_V(t'')dt''} |v'\rangle = e^{-i\int_{t'}^{t} E(t'')dt''} |v' - A(t') + A(t)\rangle = e^{-i\int_{t'}^{t} E(t'')dt''} |v\rangle \tag{1.15}$$

where $E(t'') = \frac{1}{2}\left(\mathbf{v} = \mathbf{v}' - \mathbf{A}(t'') + \mathbf{A}(t')\right)^2$ is the energy of the free electron at time t''.

$e^{-i\int_{t'}^{t} E(t'')dt''}$ is the action term which is the phase accumulated during the time of travel. Inserting Equation 1.15 in Equation 1.14 we get

$$\Psi(\mathbf{v},t) = -i\int_0^t dt' e^{-\frac{i}{2}\int_{t'}^{t} dt''[v - A(t'') + A(t)]^2} \langle \mathbf{v} - A(t') + A(t)|V_L(t')|g\rangle e^{iI_p t'} \tag{1.16}$$

Physically this means that if we want to calculate the amplitude of being in state $|\mathbf{v}\rangle$ at time t, we need to find the transition amplitude to the state $|\mathbf{v}'\rangle$ at birth time t',multiply it by the action term and then integrate over all the birth times.

Continuing with our analysis lets us assume the vector potential to be of the sinusoidal form

$$A(t) = \frac{E}{\omega_L}\sin\omega_L t = v_0 \sin\omega_L t \tag{1.17}$$

Then we can write at action term as

$$S_v(t,t') = \frac{1}{2}\int_{t'}^{t} dt''\left[v_x + v_0 \sin\omega_L t'' - v_0 \sin\omega_L t''\right]^2 - I_p t' + \frac{v_p^2}{2}(t-t') \tag{1.18}$$

$$v_0 = \frac{E}{\omega_L} \tag{1.19}$$

The electric field is polarized along the x direction and v_x, v_p are the components of **v** along and perpendicular to the polarization direction. Since v_p is not affected by the field, we can pull it out of the integral. Now using the Saddle Point approximation we can write

$$\frac{\partial S_v(t,t')}{\partial t'} = 0 \tag{1.20}$$

$$\frac{1}{2}\left(v_x + v_0 \sin\omega_L t - v_0 \sin\omega_L t'\right)^2 + \left(I_p + \frac{v_p^2}{2}\right) = 0 \tag{1.21}$$

$$\left(\frac{v_x}{v_0} + \sin\omega_L t - \sin\omega_L t'\right)^2 + \gamma^2 = 0 \tag{1.22}$$

$$\gamma^2 = \frac{2}{v_0^2}\left(I_p + \frac{v_p^2}{2}\right) \tag{1.23}$$

To our surprise, imposing the Saddle Point Approximation coupled with the SFA leads to Keldysh Parameter. If we set this parameter to zero we get

$$\frac{v_x}{v_0} + \sin\omega_L t = \sin\omega_L t' \tag{1.24}$$

This means that v_x is the velocity of the electron at time t, if it is born with zero velocity and is driven by the vector potential of Equation 1.17. Therefore, Saddle Point Approximation is a mathematical way of ensuring that the electron is born with zero velocity. If we were to include the Kelydysh parameter, it would make the birth time t' complex without changing the above analysis. This complex part of the birth time is attributed to the tunneling time.

1.4. Quantum Mechanical Three Step Model

Now that we have developed a mathematical foundation of Electron-Field interaction we can proceed to understand the Three Step Model. We begin with the ansatz

$$|\Psi\rangle = a(t)|0\rangle + |\varphi(t)\rangle \tag{1.25}$$

$|0\rangle$ is the bound ground state which decays exponentially as a function (see Equation ((1.3)) of time and $|\varphi(t)\rangle$ represents the continuum part [8]. The Hamiltonian of our system in Single Active Electron Approximation is

$$H(t) = -\frac{1}{2}\nabla^2 + V(\mathbf{r}) - E(t)x + I_p \tag{1.26}$$

Due to Dipole approximation the Electron-Field interaction is represented by

$$V_L(t) = -xE(t) \tag{1.27}$$

Time Dependent Schrödinger Equation continuum part of the ansatz is given by (using the orthogonality of the bound and continuum state)

$$i\frac{d|\varphi\rangle}{dt} = H_v|\varphi\rangle - E(t)xa(t)|0\rangle \tag{1.28}$$

$$H_V(t) = -\frac{1}{2}\nabla^2 + V(\mathbf{r}) - E(t)x + I_p \tag{1.29}$$

Solving for the continuum state $|\varphi(t)\rangle$ and then projecting it on the momentum state gives

$$\langle \mathbf{p} - \mathbf{A}(t)|\varphi(t)\rangle = -i\int_0^t dt' a(t')E(t')\langle \mathbf{p} - \mathbf{A}(t')|x|0\rangle e^{-iS(\mathbf{p},t,t')} \tag{1.30}$$

$$S(\mathbf{p},t,t') \equiv \int_{t'}^{t} dt''\left(\mathbf{p} - A(t'')\right)^2 + I_P(t-t') \tag{1.31}$$

Now, the next step is to calculate the dipole moment and then take its double derivative in time to calculate the dipole acceleration. Fourier transform of dipole acceleration gives the High Harmonic Spectrum. The dipole acceleration term is given by [8]

$$\ddot{x}(t) = \ddot{\zeta}(t) + \ddot{\zeta}^*(t) \tag{1.32}$$

where

$$\zeta(t) \equiv a^*(t)\langle 0|x|\varphi(t)\rangle \tag{1.33}$$

Improving the TSM from Zeroth Order to First Order:

TSM model discussed in the last section is successful in predicting the qualitative nature of the HHG spectrum. However, it overestimates the photon yield by almost two

orders of magnitude [8]. Hence we need to improve TSM to get a better quantitative understanding and prediction capability of high harmonic generation. This can be done by making corrections to the Strong Field Approximations (SFA) made in last section. This is also referred as improving SFA from Zeroth Order to First Order [8] This involves using the Ehrenfest theorem

$$\ddot{\zeta}(t) = 2^{3/2}\pi(2I_p)^{1/4}e^{i3\pi/4}\sum_n \frac{a(t_n(t))a(t)\sqrt{w(E(t_n(t)))}}{E(t_n(t))(t-t_n(t))^{3/2}}\langle 0|\partial_x V(\mathbf{r})|\mathbf{v}_n\rangle e^{-iS_n(t)} \tag{1.34}$$

This method for calculating the dipole acceleration improves TSM's accuracy to first order. Once again let's try to develop an intuitive understanding of this improvement. Firstly, in new ansatz of the wavefunction, we have taken into account the ground state depletion. Secondly, earlier we had assumed that when the electron is traveling outside the atom, it does not "see" the atomic potential. But by using Ehrenfest theorem, we account for the atomic potential. These differences change the recombination amplitude, hence changing the dipole acceleration. Detailed derivation of this idea can be found in [8] and [9].

1.5. Analyzing the HHG spectrum

Now that we have developed some understanding of the semi-classical and quantum nature of HHG, we are in a position to analyze HHG spectrum. Before we do that, we need to keep in mind that in reality the driver pulse is typically many wavelengths long. The electron that gets ionized after the peak of the electric field comes back to the atom half-time period later. In Figure 6, the top pulse is color coded to show the time of birth and the lower pulse shows the respective time of arrival (for instance all the electrons born in the red strip of the top pulse come back to the atom in the red strip of the lower pulse).

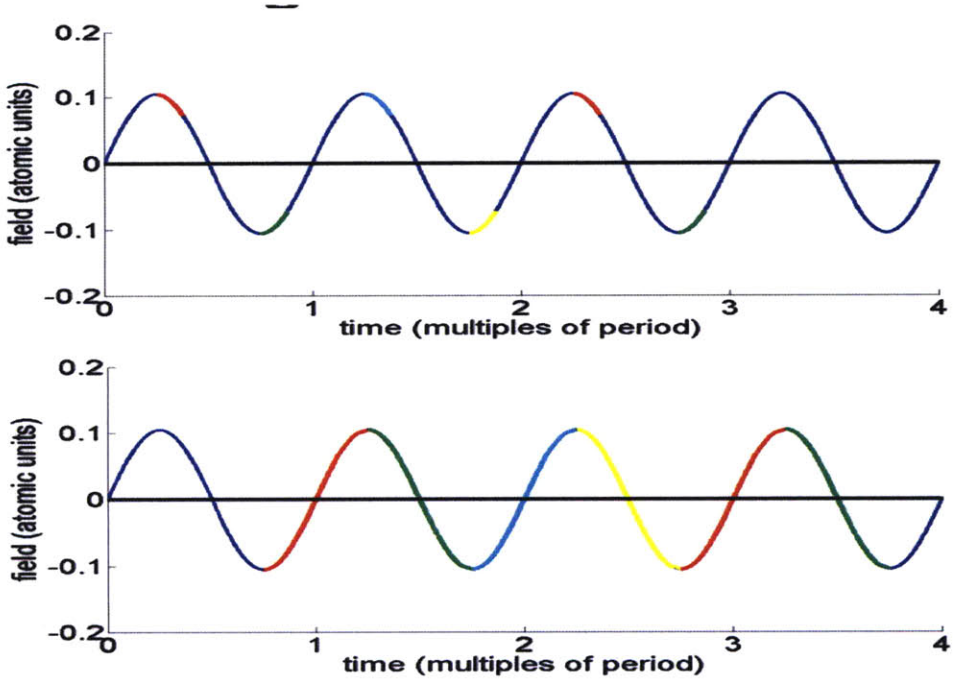

Figure 6: This Figure shows the range of recombination time and the corresponding birth time (mapped by color). This Figure was produced by V.M. Gkortsas.

So we have a burst of photons every half cycle. Fourier properties dictate that spectrum of such a signal consists of only odd harmonics. Mathematically, if a periodic function is of the form in Equation 1.35, then it will have only odd Fourier components. However, it should be noted that condition in Equation 1.35 is not true when we have a strong driving field because of ground state depletion breaks the symmetry.

$$x(t) = -x(t + \frac{T}{2}) \tag{1.35}$$

Also, since the highest harmonic is determined by the most energetic returning electron (with cut-off energy), we expect a sharp cut-off in the spectrum. These features can be observed in Figure 7. The middle section of the spectrum, where the harmonics are more or less of the same intensity is called the plateau. There are two classical trajectories: long and short, that come back to the atom with the same ponderomotive energy. The long trajectory has an earlier birth time than the short trajectory and a later arrival time (See Figure 9). As we saw in the quantum treatment of this problem, the information of the distance traveled by the

electron is stored in the action term (see Equation (1.31)). Hence, every harmonic that is generated (except the one corresponding to the longest path: brown line of Figure 4) has two different recombination events at different times. This creates a chirp in the high harmonic pulse. The long trajectories have a negative chirp and the short trajectories have a positive chirp (See Figure 8). It should also be noted, that if we use a single cycle pulse, we will not get harmonics and the spectrum is smooth with undulated cut-off. This radiation spectrum is also referred to as Bremsstrahlung term [10].

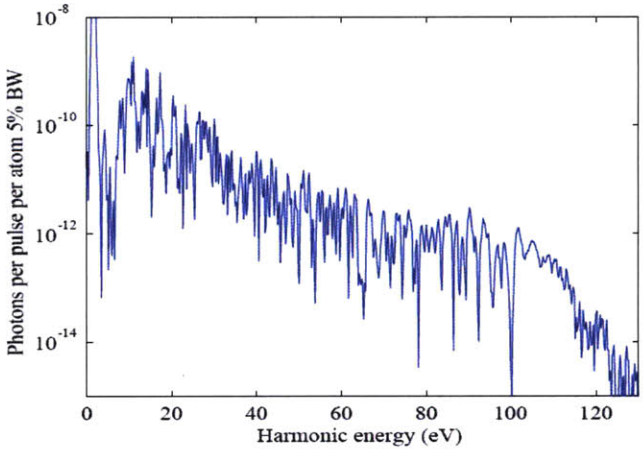

Figure 7: Simulated HHG spectra for hydrogen excited by Ti:sapphire (800nm) secant hyperbolic pulse, 5fs FWHM duration, and maximal field amplitude of 0.12au. This Figure was taken from [6].

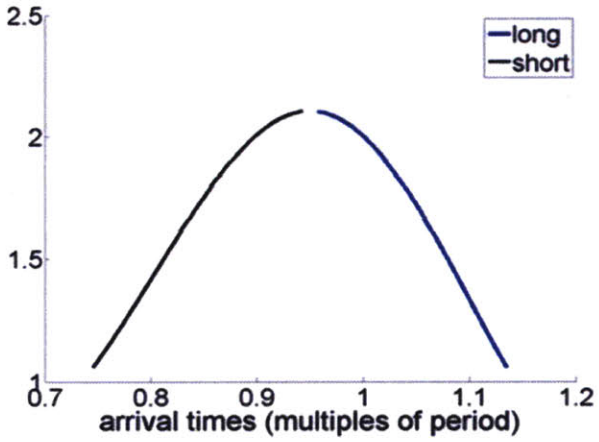

Figure 8: Energy as a function of the arrival time. Slope of the energy gives the chirp. The break in the centre represents the unique most energetic trajectory. This Figure was generated by V.M. Gkortsas

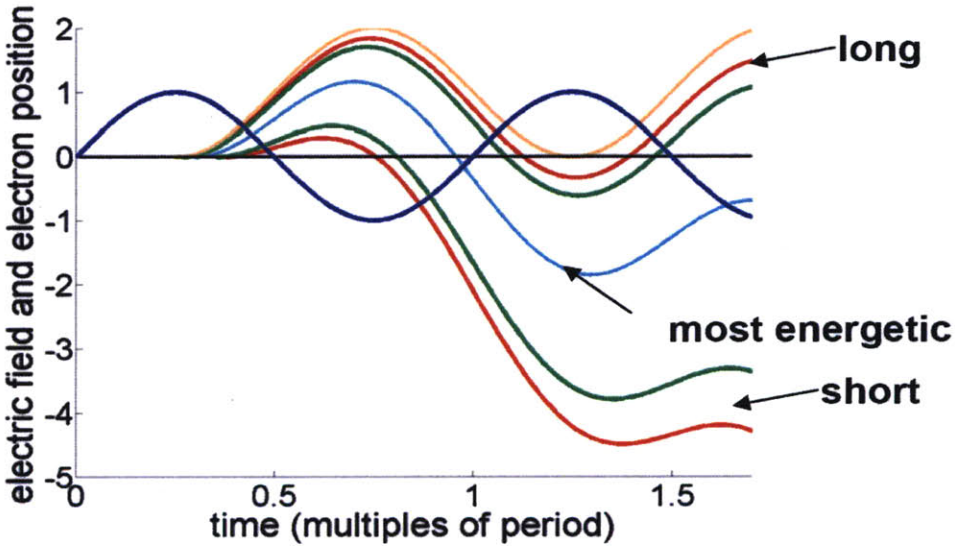

Figure 9: This Figure shows that for any given harmonic energy (except the most energetic one), we have two classical trajectories. This Figure was produced by V.M. Gkortsas.

1.6. Solving Time Dependent Schrödinger Equation numerically

The Three Step Model, is a great tool to understand HHG. However, it does not always predict the high harmonic spectrum accurately. For example, it is based on Strong Field Ionization which assumes that electron is born with zero velocity via tunneling. But as mentioned earlier, there can be other channels of ionization like Multi-Photon ionization which are not accounted for by TSM. As mentioned before, Multi-photon ionization can become important when we are pushing for driver pulses of low intensity or short wavelength.

Secondly, even the improved TSM Equation assumes that the electrons wave packet returns back only once to the atom. However, this is not the case, and electrons that have not recombined can either get re-scattered or comeback at a later time to recombine.

Thirdly, numerical simulation is a good way to check the robustness of theories like TSM. Sometimes, it may also lead to the discovery of some phenomena that might have been overlooked in earlier theories. For instance, we found that in addition to the harmonics that are separated by twice the driving frequency, there was an additional longer modulation on the HHG spectra. We believe that this is due to quantum interference between the returning electronic wave packet and the one that is emerging from the atom.

2. Numerical Time Dependent Schroedinger Equation

2.1. Introduction

In this chapter the numerical technique used to solve the Time Dependent Schroedinger Equation for hydrogen atom will be discussed. This scheme can be divided into two broad parts, namely

a) Discretization of Hamiltonian and
b) Propagating the wavefunction in time.

The program uses Asyptotic Behavior Correspondence (ABC) discretization in space and Leap frog method for time propagation [11]. This is a second order finite difference scheme for solvng the Time-dependent Schroedinger Equation of the ground state of the Hydrogen atom:

$$i\frac{\partial|\Psi\rangle}{\partial t}=\left[-\frac{\nabla^2}{2}-\frac{1}{r}-zE(t)\right]|\Psi\rangle \tag{2.1}$$

The first two terms of the Hamiltonian represent the kinetic energy and potential of the hydrogen atom, while the last term is the interaction of the system with the electric field. This interaction is obtained by using dipole approximation in length gauge. This approximation assumes that the distance that the electron travels from the atom is much smaller than the driver's wavelength. More on this approximation will be discussed in Chapter 4.

2.2. Discretization in Space

The presence of coulomb singularity can make the discretization of space for our problem a tricky affair. Smoothing the singularity is commonly used to circumvent this problem. This involves replacing $\frac{Z}{r}$ by either $\frac{Z}{r+a}$ [12] or $\frac{Z}{\sqrt{r^2+a^2}}$ [13]. However, smoothing the

singularity can alter the results of HHG by orders of magnitude to give the correct photon yield. This is because of the different analytic behavior of the potential close to the origin is critical to the calculation of recombination amplitude [14] By TSM, the amplitude of the emitted radiation is proportional to the double derivative in time of the recombination amplitude [15] It has been shown that calculating the recombination amplitude from a plane wave to the ground state is equivalent to finding the Fourier transform of the first excited state [14].

$$a_{rec}(\mathbf{k}) = \langle 0|x|\mathbf{k}\rangle = \frac{1}{(2\pi)^{3/2}} \int \psi_o^*(\mathbf{r}) x e^{i\mathbf{k}.\mathbf{r}} d^3r \tag{2.2}$$

Fourier Transform of a function is sensitive to the discontinuities in the derivative of the function. In the absence of any derivative discontinuity, the transform decays exponentially for large $\mathbf{k}$. If a discontinuity is present, the transform decays like a power law whose exponent is determined by the order of the derivative in which the discontinuity is present [14]. Since the coulomb singularity is responsible for the discontinuity in the first derivative of the wave function, it is important that we treat it carefully.

The method used in our code is called Asymptotic Behavior Correspondence (ABC) in cylindrical co-ordinate system [11]. Cylindrical co-ordinate system is used because it helps us reduce a 3D problem to a 2D problem due to symmetry around the azimuthal angle. The main idea of ABC is that we know the analytic behavior of the wave function close to the singularity. Lets us see how this idea works. In cylindrical co-ordinate laplacian is given by

$$\Delta f = \frac{\partial^2 f}{\partial^2 \rho} + \frac{1}{\rho^2}\frac{\partial^2 f}{\partial^2 \theta} + \frac{1}{\rho}\frac{\partial f}{\partial \rho} + \frac{\partial^2 f}{\partial^2 z} \tag{2.3}$$

Let $f = \frac{g}{\sqrt{\rho}}$ and dropping the azimuthal dependence we can write

$$\frac{\partial f}{\partial \rho} = \frac{1}{\sqrt{\rho}}\frac{\partial g}{\partial \rho} - \frac{1}{2\rho^{3/2}} g \tag{2.4}$$

$$\frac{\partial^2 f}{\partial^2 \rho} = \frac{1}{\sqrt{\rho}}\frac{\partial^2 g}{\partial^2 \rho} - \frac{1}{\rho^{3/2}}\frac{\partial g}{\partial \rho} + \frac{3}{4\rho^{5/2}} g \tag{2.5}$$

Inserting the above two equations into the laplacian of f we get

$$\sqrt{\rho}\Delta f = \frac{\partial^2 g}{\partial \rho^2} + \frac{1}{4\rho^2} g \tag{2.6}$$

Now lets look for eigenfunction of f such that

$$-\Delta f = \lambda f \Rightarrow -\sqrt{\rho}\Delta f = \sqrt{\rho}\lambda f \Rightarrow -\Delta g = \lambda g \tag{2.7}$$

Bessel function of the first kind J_0 satisfies the eigenvalue equation of f. Expanding J_0 around the origin we get

$$g(\rho) = \sqrt{\rho} + O(\rho^{5/2}) \tag{2.8}$$

Modified laplacian of g can be written in second order finite difference scheme as

$$\Delta g = \frac{g_{j+1} + g_{j-1} - 2g_j}{\delta^2} + \frac{g_j}{4j^2\delta^2} \tag{2.9}$$

Now according to ABC, insert the asymptotic form of g into the above equation and use the eigenvalue Equation (2.7), to get

$$\Delta g = \frac{g_{j+1} + g_{j-1} - 2g_j}{\delta^2} + \frac{c_j g_j}{4\delta^2} \tag{2.10}$$

$$c_j = 8 - 4\sqrt{1+\frac{1}{j}} - 4\sqrt{1+\frac{1}{j}} \tag{2.11}$$

Note that as $j \to \infty, c_j \to \frac{1}{j^2}$. So far away from the origin, ABC discretization is the same as normal discretization. Now lets return to our Hamiltonian which in cylindrical co-ordinate system, along with the transformation $\phi(\rho, z) = \sqrt{\rho}\Psi(\rho, z)$, can be written as

$$H = -\frac{1}{2}\frac{\partial^2}{\partial^2 z} - \frac{1}{2}\frac{\partial^2}{\partial^2 \rho} - \frac{1}{8\rho^2} - \frac{1}{\sqrt{\rho^2 + z^2}} \tag{2.12}$$

In finite difference scheme we can write the Hamiltonian as[11]

$$[H\phi]_{jk} = -\frac{\Delta\phi_{jk}}{2\delta^2} - c_j\frac{\phi_{jk}}{8\delta^2} - \frac{q_{jk}}{\delta}\phi_{jk} \tag{2.13}$$

We have found c_j before. q_{jk} can be found by asymptotic expansion of ϕ_{jk} near the origin:

$$\phi_{jk} = \sqrt{j}\left(1 - Z\delta\sqrt{j^2 + k^2} + b_z\delta k\right) \tag{2.14}$$

Details of this expansion can be found in [11]

2.3. Calculation of Ground State

Once we have set up the discreet Hamiltonian, next step is to find the ground state. Ground state is found using the Imaginary Time Propagation (ITP) method [16]. This means we map time $t \to -i\tau$ and propagate a random guess for ground state using the Schrödinger equation in imaginary time

$$\frac{\Psi(\mathbf{r},\tau)}{d\tau} = -H\Psi(\mathbf{r},\tau) \tag{2.15}$$

We can start with a random guess for the initial state $\Psi(\mathbf{r},0)$ which can be written as the superposition of the eigenstates of the Hamiltonian

$$\Psi(\mathbf{r},0) = \sum c_i \psi_i \tag{2.16}$$

Plugging the above equation in Equation (2.15) we get the time evolution of each eigenstate:

$$\psi_i(\tau) = e^{-\tau E_i}\psi_i(0) \tag{2.17}$$

Ground state has the smallest energy and hence the higher eigenstates decay exponentially faster by:

$$\frac{\psi_i(\tau)}{\psi_0(\tau)} = e^{-\tau(E_i - E_0)}, \tag{2.18}$$

$$\Psi(\mathbf{r},\tau) = \sum c_i e^{-\tau E_i}\psi_i(0) \tag{2.19}$$

2.4. Propagation in Time

Once we have found the discreet ground state, the next step is to propagate this state in time in the presence of the perturbative electromagnetic field. The Schrödinger equation is a Parabolic Partial differential equation. There are several techniques to march the solution of a Parabolic PDE in time. They can be divided into two broad categories:

a) **Implicit Schemes**: These schemes are unconditionally stable but can be numerically expensive because they involve matrix inversion. Examples of Implicit schemes are Crank Nicolson and Backward Euler.

b) **Explicit Schemes**: These schemes have conditionally stable and relatively inexpensive numerically. However, due to conditionally stability one needs to carefully choose time and space discretization so that the simulation does not blow up with the number of time iterations. Examples of Explicit schemes are Forward Euler and Leapfrog method. For our numerical simulation we use the latter.

To better understand the Leapfrog method lets re-write the Schrödinger equation

$$\partial_t \Psi = -i\hat{H}\Psi \tag{2.20}$$

Expanding the wave function in the eigenstates: $\Psi(t) = \sum c_j(t) u_j$, we can write the Schrödinger equation for each eigenstate as:

$$\partial_t c_j(t) = -iE_j c_j(t) \tag{2.21}$$

$$c_j(t) = c_j(0) e^{-iE_j t} \tag{2.22}$$

In discreet form Schrödinger equation of each eigenstate can be written as:

$$\frac{c^{n+1} - c^{n-1}}{2\Delta t} = -iEc^n \tag{2.23}$$

This is a second order accurate scheme. Superscript n is the represented the time step. To calculate the time step $n+1$, we apply the Hamiltonian on the time step n. That is why this scheme is called the Leapfrog method. Let us now look at the stability condition of Leap frog method. We begin by defining the time propagation operator S:

$$Sc^n = c^{n+1} \tag{2.24}$$

The characteristic of the discreet time evolution can be written as:

$$\{S^2 + 2i\Delta t ES - 1\} c^n = 0 \tag{2.25}$$

The roots of this characteristic equation are:

$$\sigma_{1/2} = -iE\Delta t \pm \sqrt{1 - (E\Delta t)^2} \tag{2.26}$$

The two roots of the characteristic equation are:

$$\sigma_1 = -iE\Delta t + 1 - \frac{(E\Delta t)^2}{2} - \frac{(E\Delta t)^4}{8} \ldots\ldots \tag{2.27}$$

$$\sigma_2 = -iE\Delta t - 1 + \frac{(E\Delta t)^2}{2} + \frac{(E\Delta t)^4}{8} \ldots\ldots \tag{2.28}$$

Of the two solutions only σ_2 (Equation (2.28)) is stable. For the time evolution to be stable, $|\sigma_{1/2}| < 1$. In other words $E\Delta t < 1$. Hence, largest eigenenergy in the simulation determines the optimum time step. For example, in our simulation, the largest energy is the cut-off and therefore the time step should be smaller than inverse of cut-off.

In Equation (2.23), we learnt how to handle the time discretization. Numerically, one can calculate the eigenenergy, by matrix vector multiplication: the Hamiltonian is represented by a matrix and the eigenstate by a vector. Let us see how this works for the simple case when there is no potential and the Hamiltonian consists of only kinetic energy term. Its well known that kinetic energy or double derivative is represented by a tri-diagonal matrix:

$$A = \begin{bmatrix} -2 & 1 & & & \\ 1 & -2 & 1 & & 0 \\ & \ddots & \ddots & \ddots & \\ & & \ddots & \ddots & 1 \\ 0 & & & 1 & -2 \end{bmatrix}$$

Equation (2.23) can be re-written as:

$$\vec{\Psi}^{n+1} - \vec{\Psi}^{n-1} = -i\frac{2\Delta t}{\Delta x^2} A\vec{\Psi}^{n} \tag{2.29}$$

Eigenvalues of tri-diagonal matrix with diagonal b and off-diagonal a is given by

$$E_j = b + 2a\cos(\frac{j\pi}{N}) \tag{2.30}$$

The above equation along with $E\Delta t < 1$ gives the stability condition:

$$\frac{4\Delta t}{\Delta x^2} < 1 \tag{2.31}$$

2.5. Conclusion

To summarize, we choose cylindrical co-ordinate system due to symmetry and simplify the laplacian by the transformation $f = \frac{g}{\sqrt{\rho}}$. To handle the singularity we employ the ABC discretization. Then the ground state is found by propagating in imaginary time. Once we have the ground state, we use the leap frog method along with stability condition to propagate the solution in time. We need to normalize the wavefunction after every few time steps. In order to prevent any reflection form the boundaries, absorbing boundary conditions have been employed.

3. Results from NTDSE Simulations

3.1. Comparison between TSM spectra and NTDSE spectra

In this section, harmonic spectra produced by NTDSE and TSM are compared for different electric fields. Ionization potential of Hydrogen is about $13 e.v.$ The harmonics that appear below this energy are caused by traditional non-linear processes. In fact, the first harmonic peak of the NTDSE simulation is at the frequency of the driving field. This harmonic is not present in TSM spectra. In Figure 10 $(\gamma = 0.475)$, TSM and NTDSE differ by about 1-2 orders of magnitudes deep in the plateau region. In Figure 11 $(\gamma = 0.57)$, TSM and NTDSE differ by about 2-3 orders of magnitudes deep in the plateau region. In Figure 12 $(\gamma = 0.95)$, TSM and NTDSE differ by about 3-4 orders of magnitudes. These results agree with the theory discussed in Chapter 1: as the value of Keldysh Parameter decreases, TSM becomes more valid. However, close to the cut-off, TSM and NTDSE differ by only an order of magnitude in all the cases.

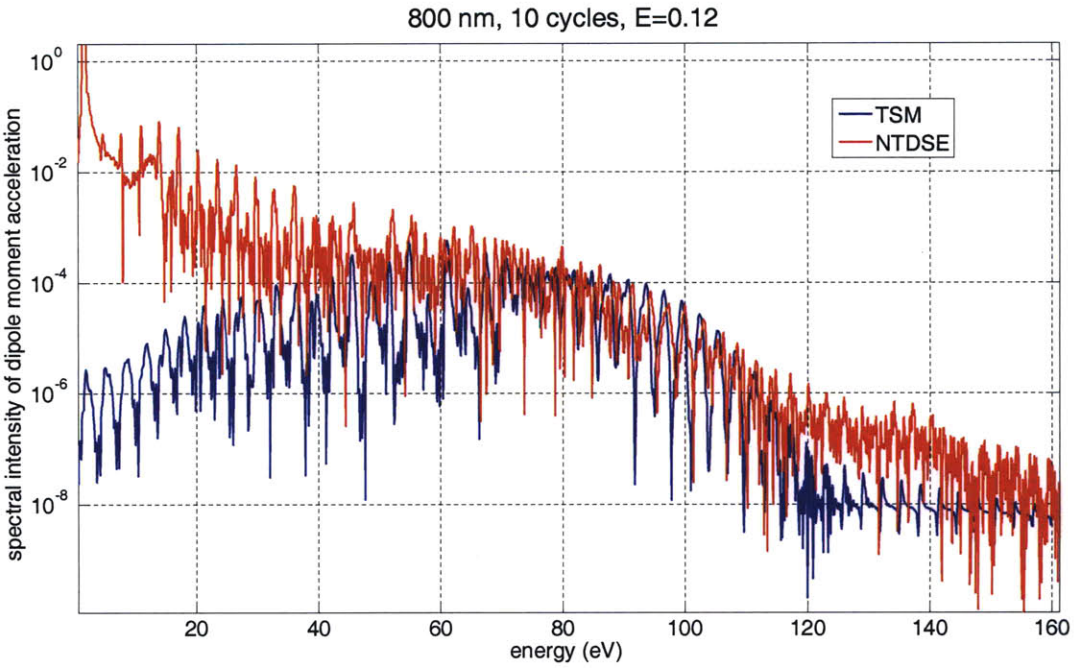

Figure 10: Comparison between TSM (blue) and NTDSE spectra for 800 nm, 10 cycle pulse with peak electric field E= 0.12 atomic units

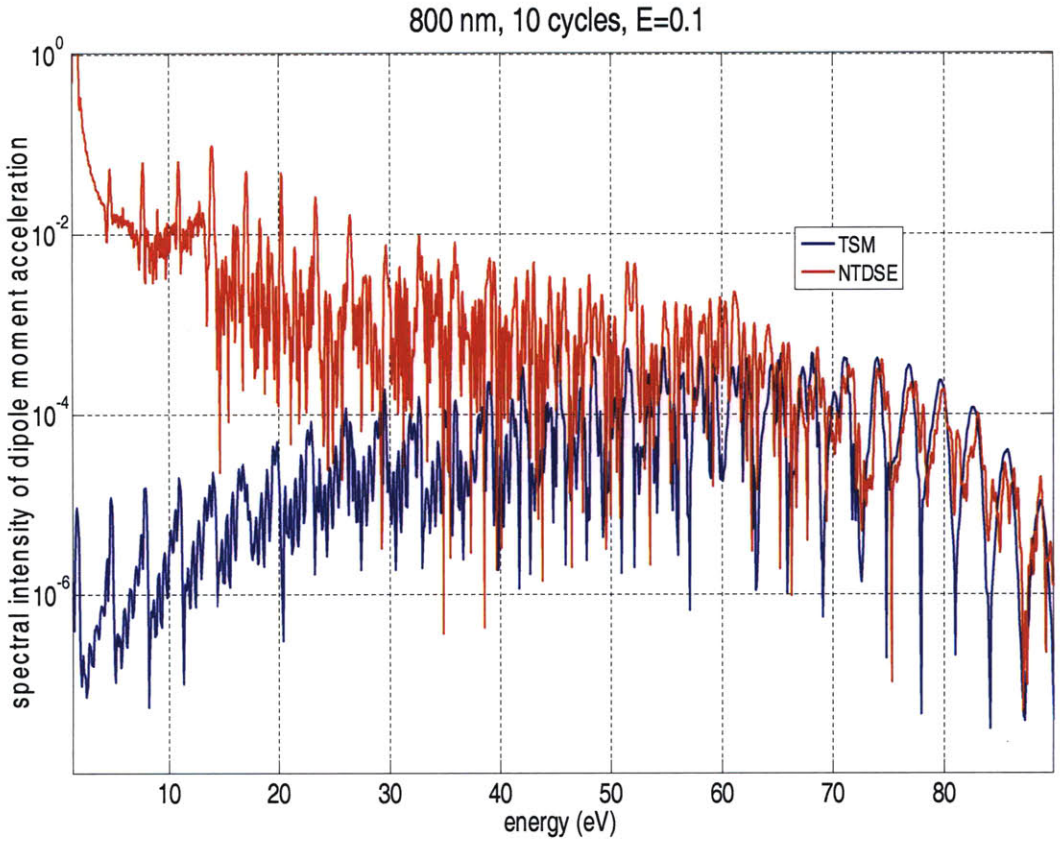

Figure 11: Comparison between TSM (blue) and NTDSE spectra for 800 nm, 10 cycle pulse with peak electric field E= 0.10 atomic units

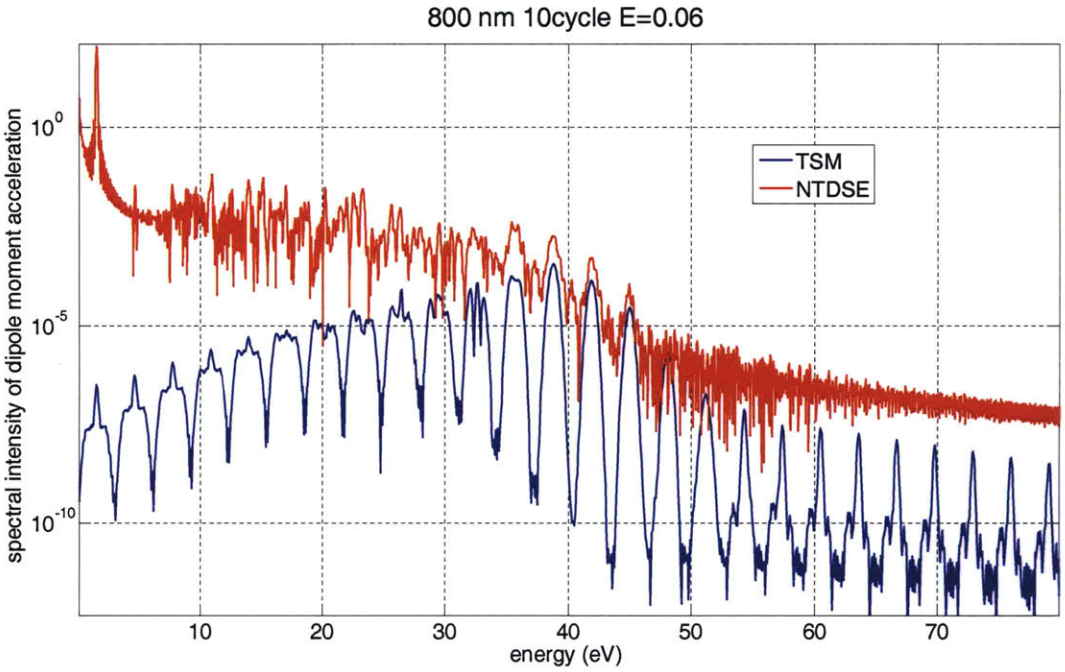

Figure 12: Comparison between TSM (blue) and NTDSE spectra for 800 nm, 10 cycle pulse with peak electric field E= 0.06 atomic units

3.2. Interaction of Hydrogen with 800 nm pulse

Here we look at the interaction of Hydrogen with 800 nm pulses which are of varying cycles and electric fields. Our aim here is to find, the optimum electric field and the number of cycles that maximizes the efficiency of single atom response of energy radiated in any given harmonic frequency. Efficiency of single atom response is defined as the ratio of energy radiated in a given harmonic and the total energy in the driver pulse. It should be noted that the frequency of the harmonics does not change when the electric field is changed. Energy radiated in a given frequency is calculated by integrating from $-\omega_0$ to ω_0 around that frequency. For our purposes, three trial electric fields have been chosen:

	Case 1	Case 2	Case 3
Electric Field (a.u.)	0.06	0.08	0.12
Cut-off (e.v.)	37.49	56.08	109.17
Keldysh Parameter	0.95	0.7125	0.475

Figure 13 is the spectrum for $E = 0.08 a.u.$, 10 cycles. As expected, we can observe odd harmonics separated by $2\omega_0 = 3.102 e.v.$. The first peak is at the driving field frequency. The ionization potential is $13.5 ev$ and the harmonics with frequency below the ionization potential are produced by the traditional non-linear processes explained by Drude Model.

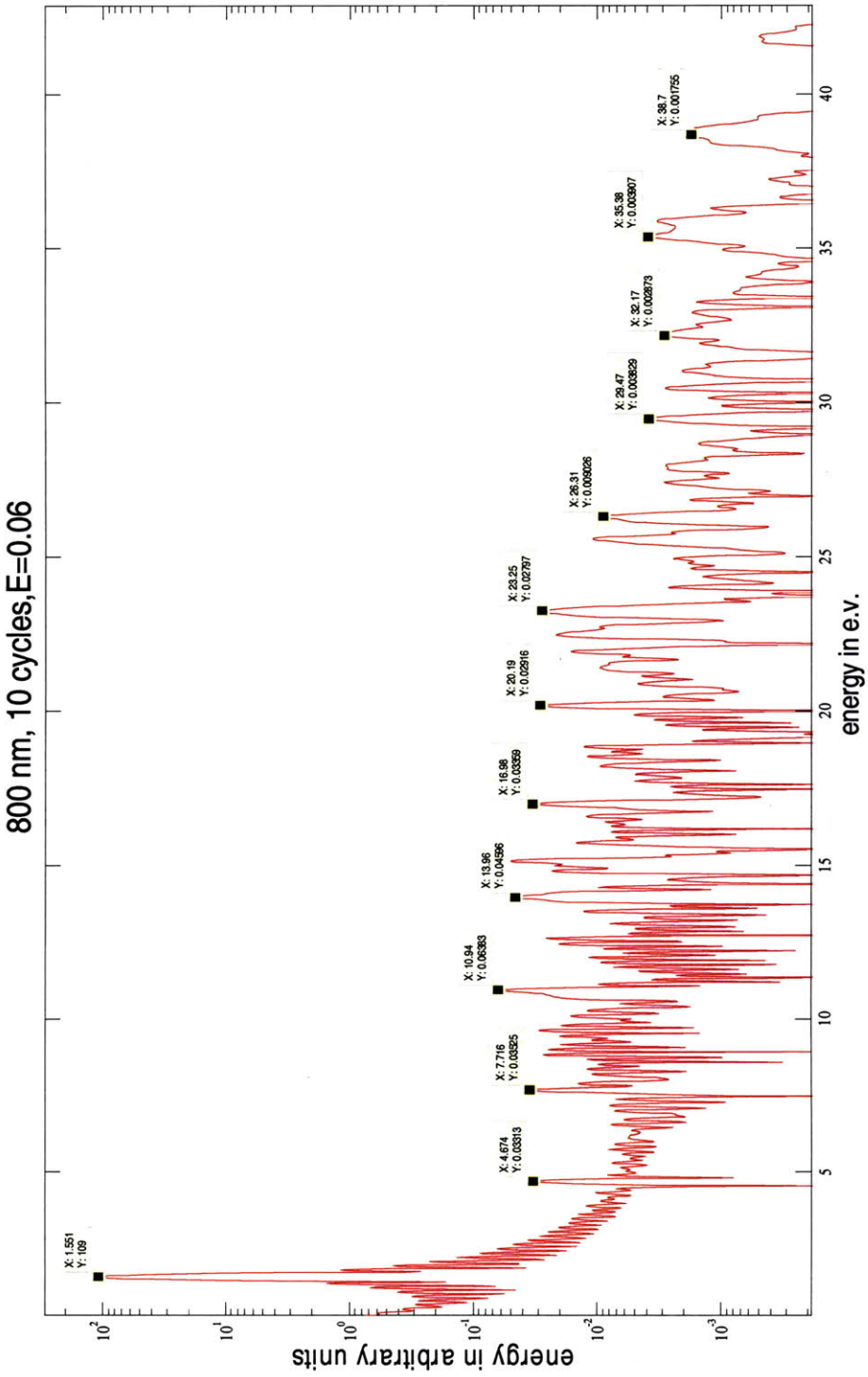

Figure 13: Energy spectrum of 800nm driver pulse. As expected, we observe odd harmonics separated by twice the driving frequency

Figure 14 to Figure 24 are the plots of efficiencies for different harmonics for three electric fields: $E = 0.06, E = 0.08$ and $E = 0.12$ (all the electric fields are in atomic units) Harmonics in the plateau region, have the highest efficiencies when the driver field is a few cycles long (4-10 cycles) and with $E = 0.08$. As we move closer to the cut-off, driver pulses of smaller electric field ($E = 0.06$) and large number of cycles produce the best efficiencies Note that strong electric field driver pulses ($E = 0.12$) have low efficiency for all harmonics. This is because the driver depletes the ground state very quickly and the recombination amplitude is very small. Depletion of ground state for $E = 0.06, E = 0.08$ and $E = 0.12$ is shown in Figure 25, Figure 26 and Figure 27 respectively.

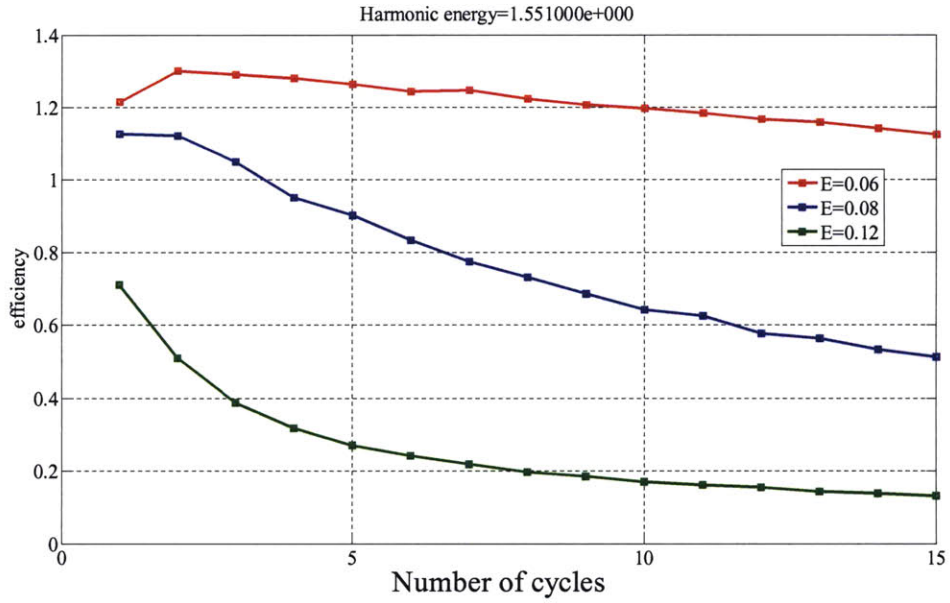

Figure 14:First Harmonic of 800nm driver pulse: 1.55 e.v.

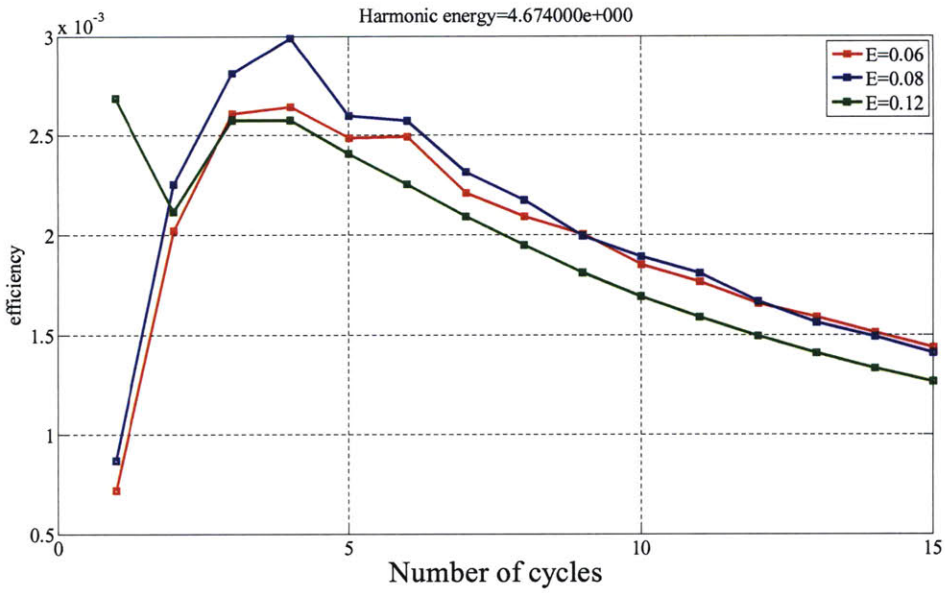

Figure 15: Third Harmonic of 800nm driver pulse: 4.67 e.v.

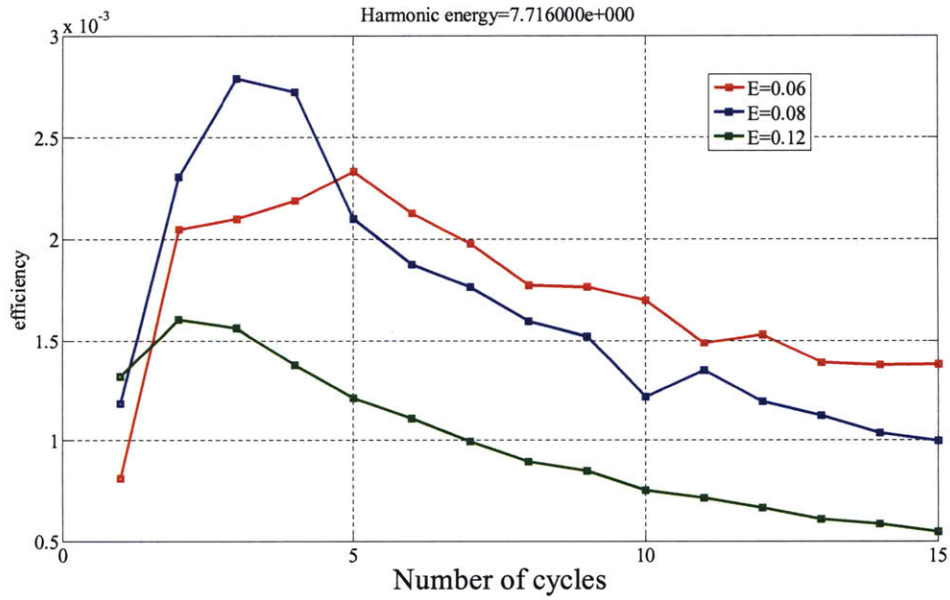

Figure 16: Fifth Harmonic of 800nm driver pulse: 7.71 e.v.

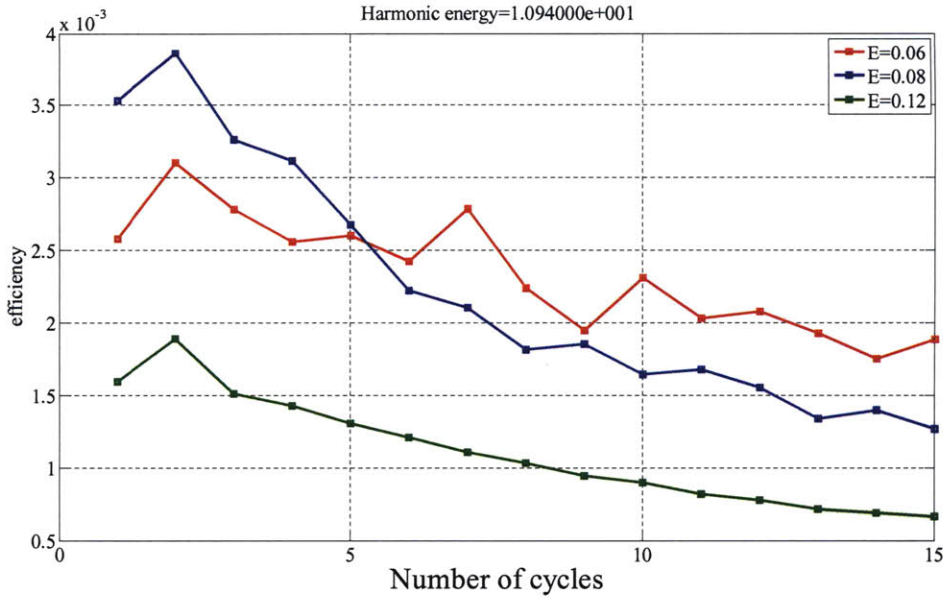

Figure 17: Seventh Harmonic of 800nm driver pulse: 10.94 e.v.

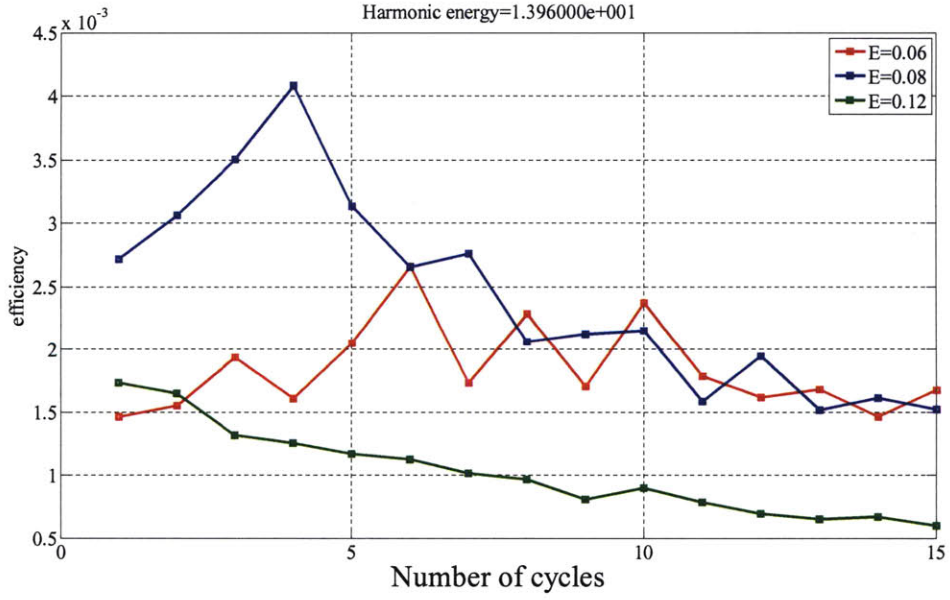

Figure 18: Ninth Harmonic of 800nm driver pulse: 13.96 e.v.

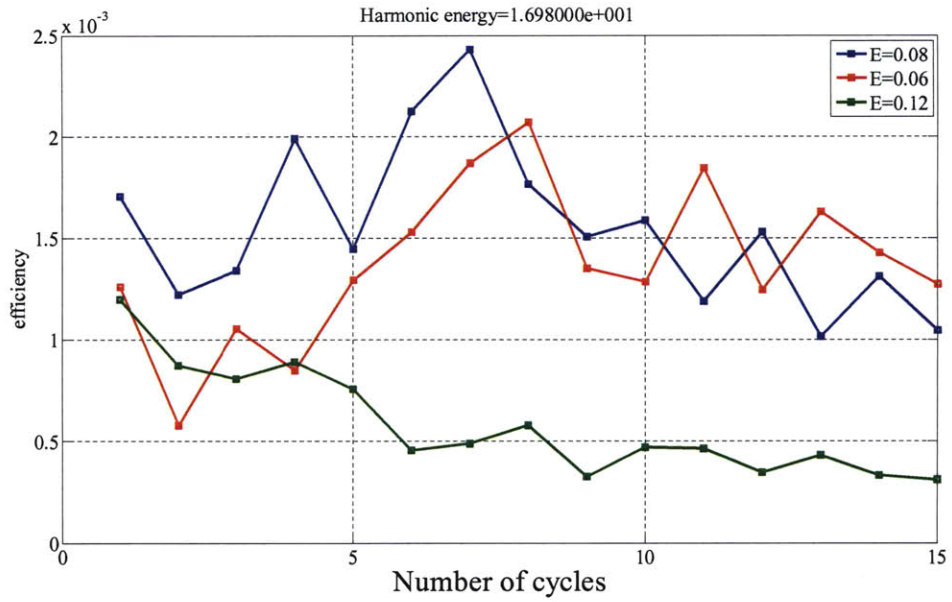

Figure 19: Eleventh Harmonic of 800nm driver pulse: 16.98 e.v.

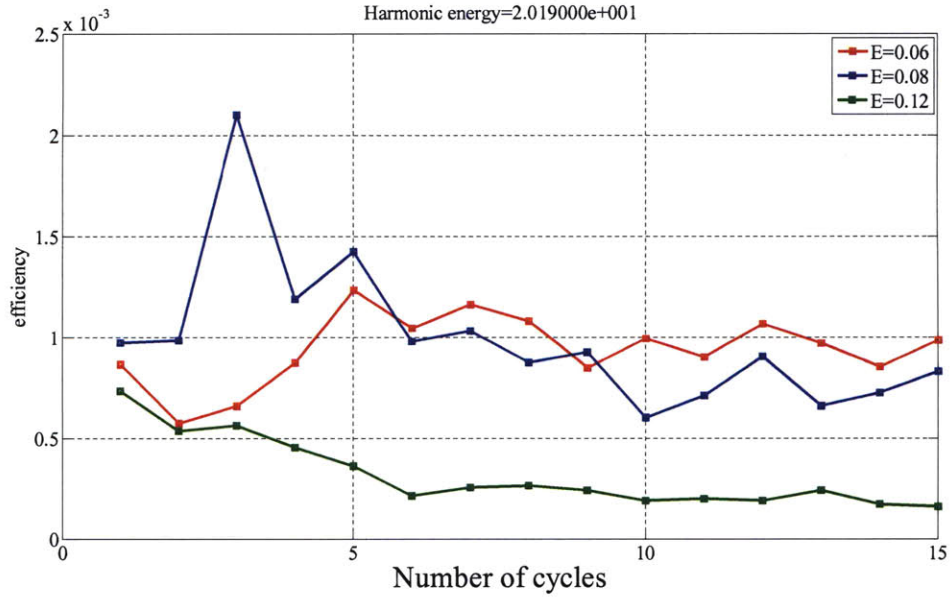

Figure 20: Thirteenth Harmonic of 800nm driver pulse: 20.19 e.v.

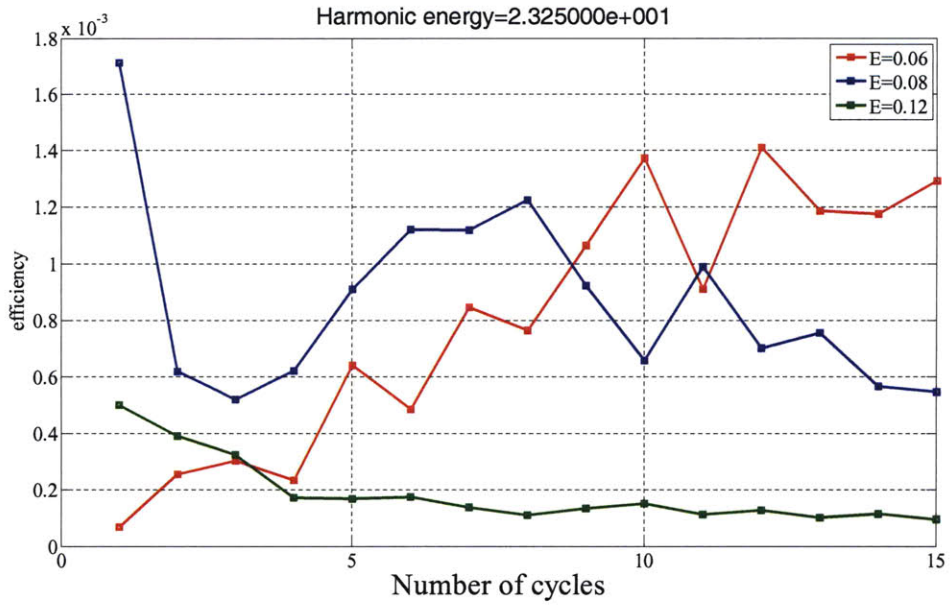

Figure 21: Fifteenth Harmonic of 800nm driver pulse: 23.25 e.v.

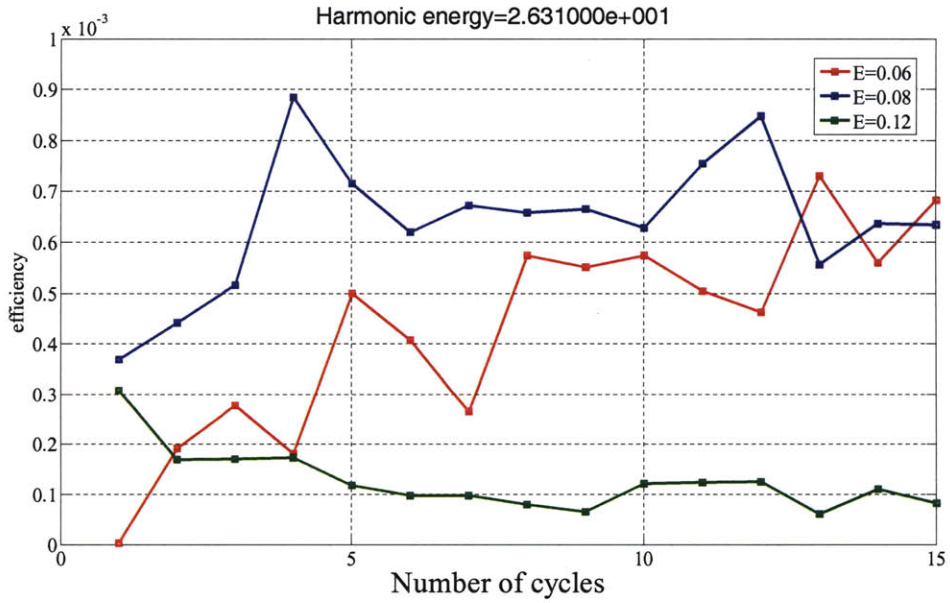

Figure 22: Seventeenth Harmonic of 800nm driver pulse: 26.31 e.v.

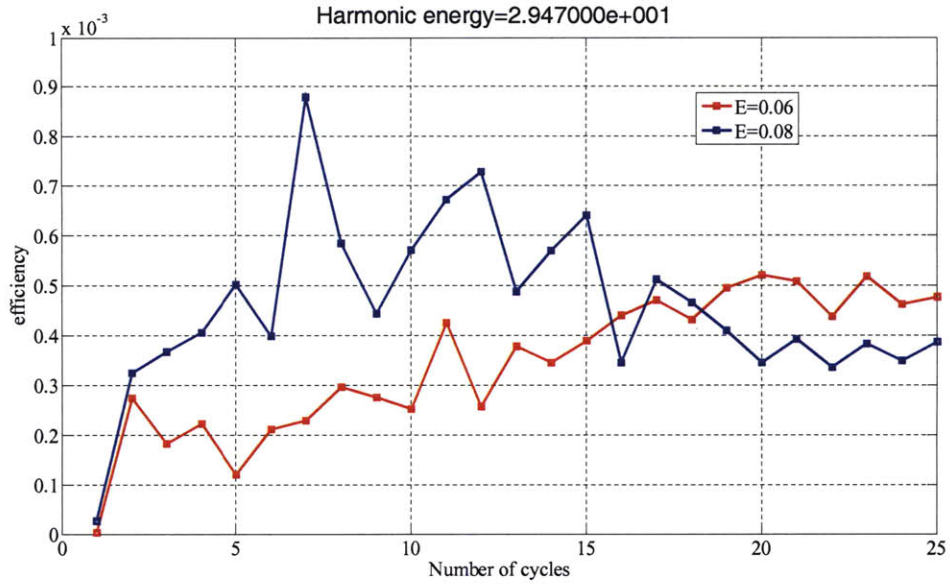

Figure 23: Nineteenth Harmonic of 800nm driver pulse: 29.47 e.v.

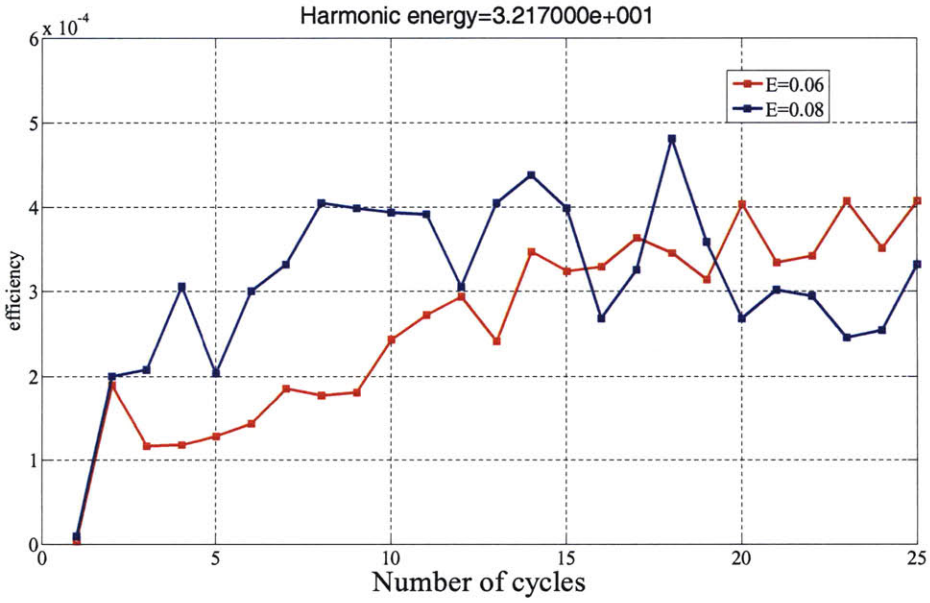

Figure 24: Twenty first Harmonic of 800nm driver pulse: 32.17 e.v.

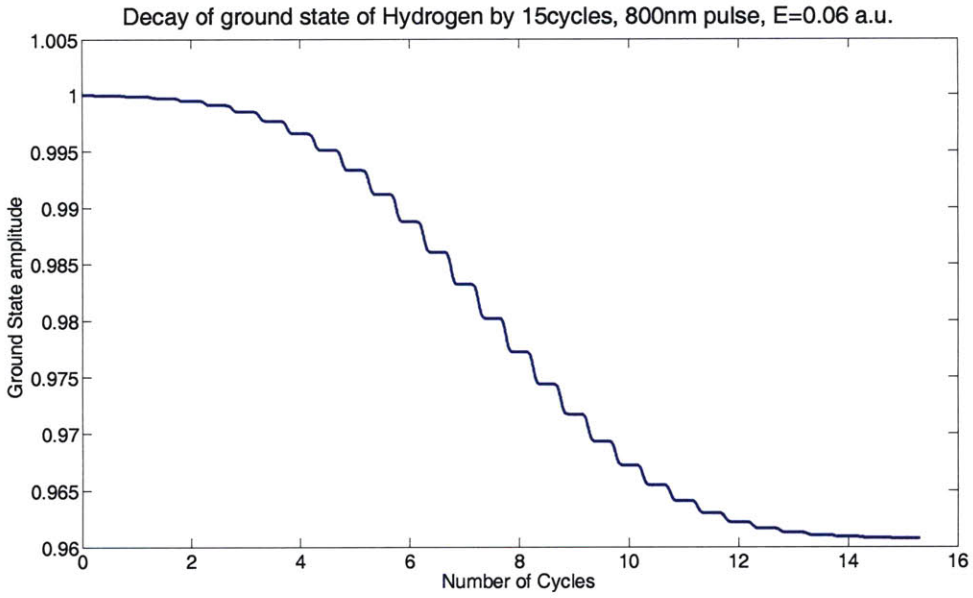

Figure 25: Ground state decay calculated by ADK formula for 800 nm,10 cycle pulse with E=0.06

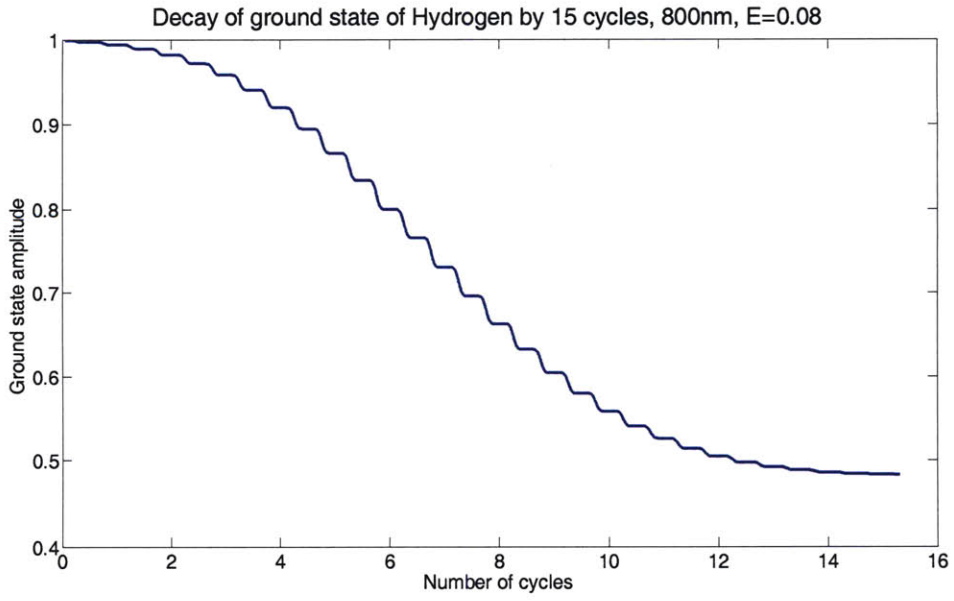

Figure 26: Ground state decay calculated by ADK formula for 800 nm,15 cycle pulse with E=0.08

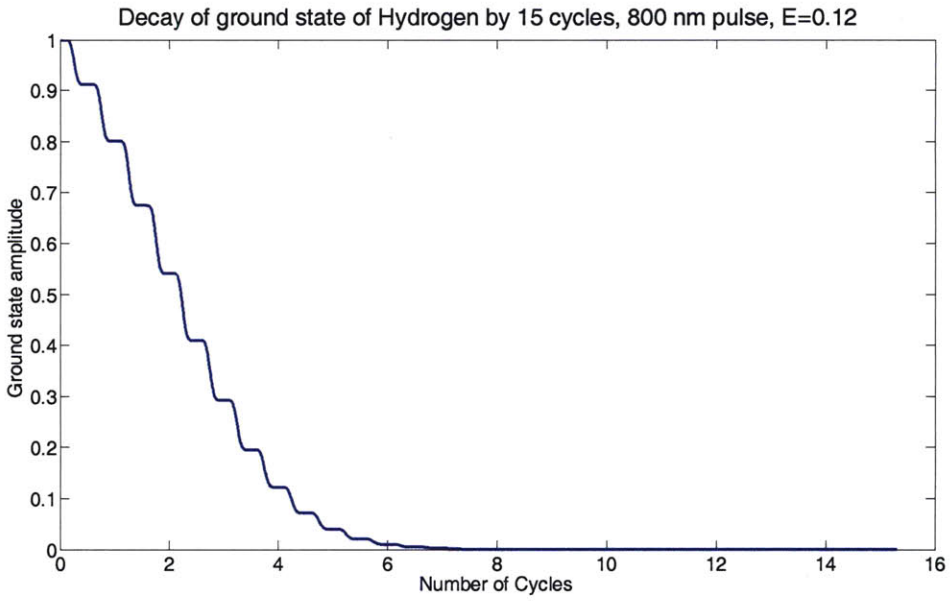

Figure 27: Ground state decay calculated by ADK formula for 800 nm,15 cycle pulse with E=0.12

3.3. Interaction of Hydrogen with 400 nm pulse

Now, like for the $800nm$ case in previous section, interaction of Hydrogen with 400 nm driver fields of varying cycles and electric fields is investigated. The three different cases have been summarized in the following table:

	Case 1	Case 2	Case 3
Electric Field (a.u.)	0.06	0.08	0.14
Cut-off (e.v.)	19.57	24.22	46.12
Keldysh Parameter	1.425	1.425	0.814

High Harmonic Spectrum of $10 cycles$ driver pulse with $E = 0.08 a.u.$, 10 is shown in Figure 28 As expected, odd harmonics separated by $2\omega_0 = 6.203$ *e.v.* are observed. Due to smaller wavelength, the cut-off of $400nm$ driver pulse is smaller than its $800nm$ counterpart. Also, the harmonics are further spaced for shorter wavelength. As a result, as we move towards shorter driver pulses, we observe fewer harmonics.

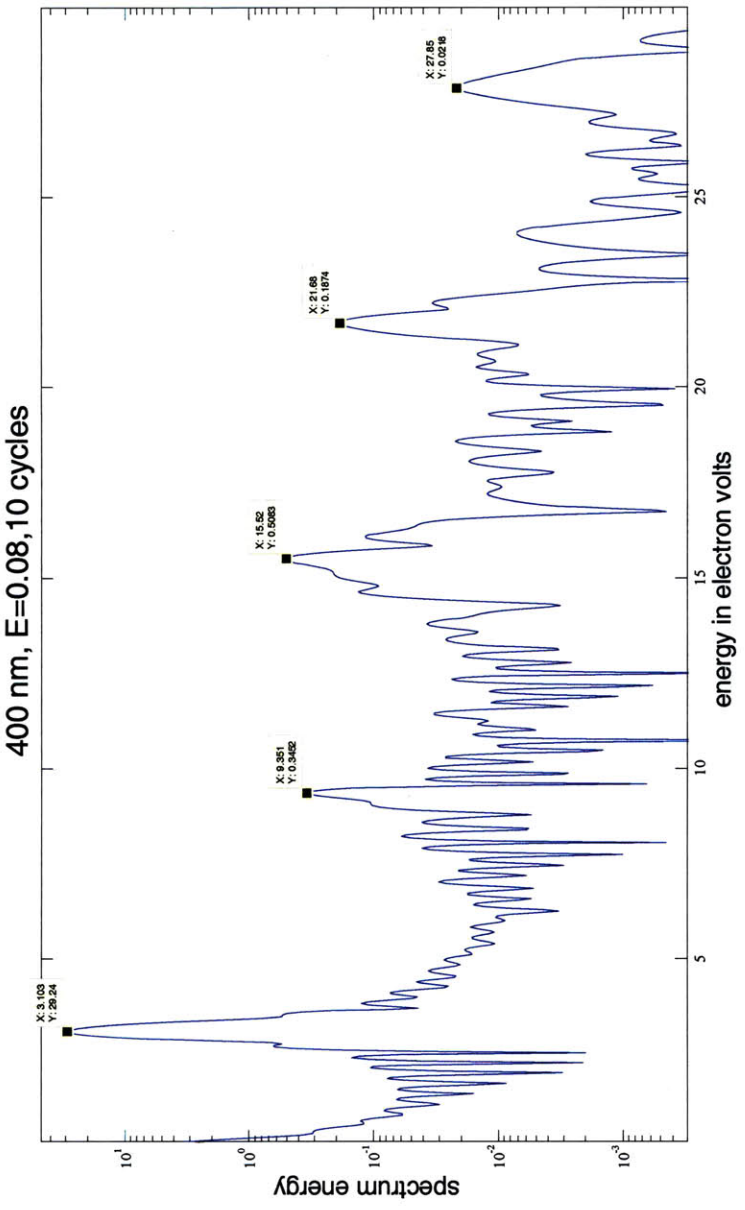

Figure 28 Energy spectrum of 400nm driver pulse. As expected, we observe odd harmonics separated by twice the driving frequency

Figure 29 to Figure 33 are plots of harmonic efficiencies of the harmonics. Figure 34 , Figure 35 and Figure 36 show the ground state decay by $E = 0.06$, $E = 0.08$ and $E = 0.14$ respectively.

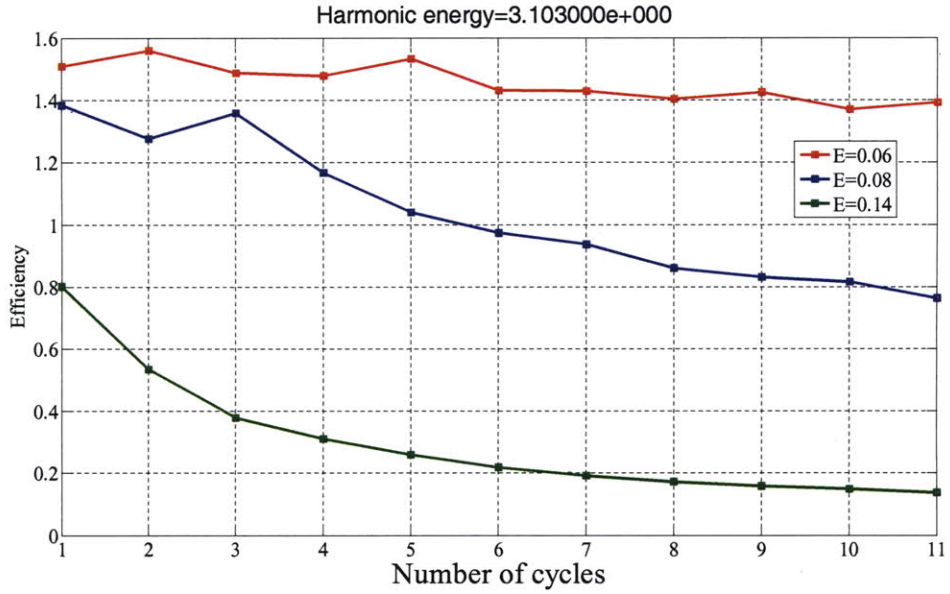

Figure 29: Harmonic efficiencies at First Harmonic of 400nm driver pulse: 31.03 e.v.

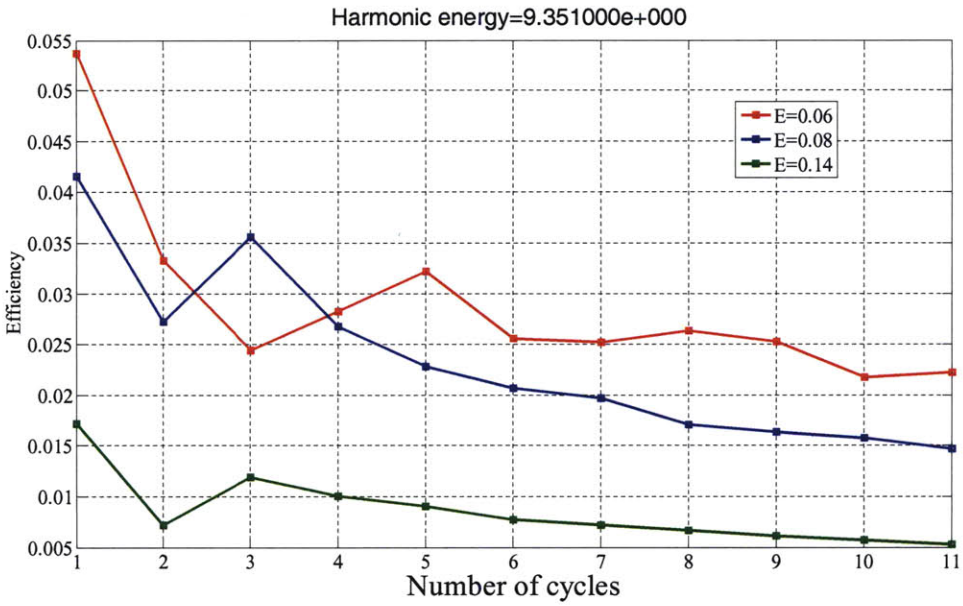

Figure 30: Harmonic efficiencies at Third Harmonic of 400nm driver pulse:9.35 e.v.

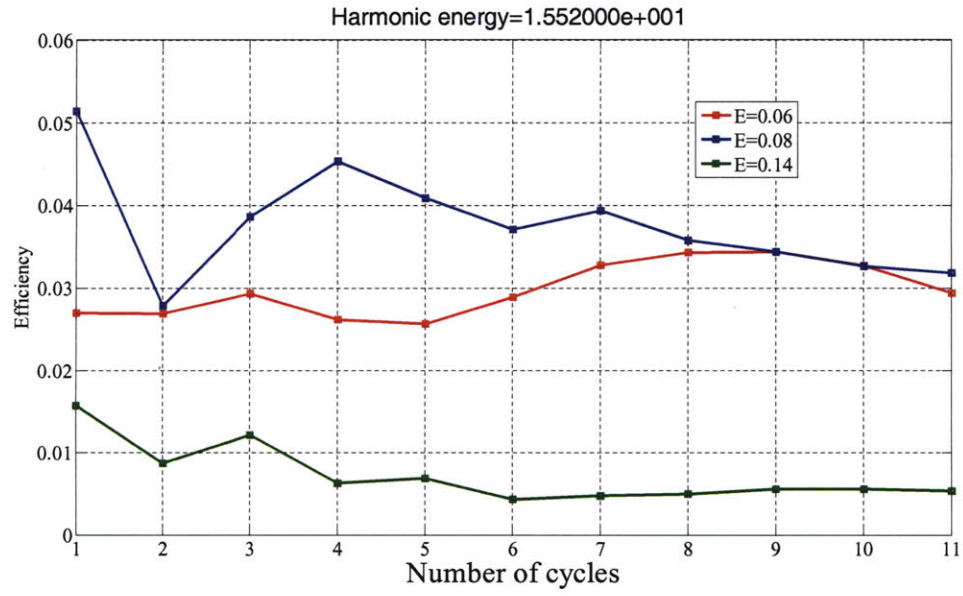

Figure 31: Harmonic efficiencies at Fifth Harmonic of 400nm driver pulse: 15.52 e.v.

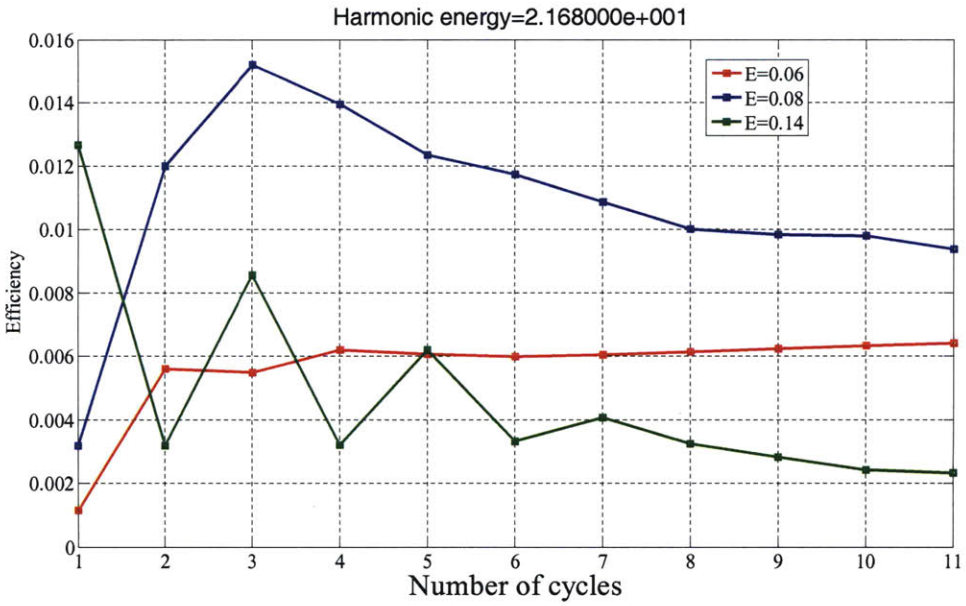

Figure 32: Harmonic efficiencies at Seventh Harmonic of 400nm driver pulse: 21.68 e.v.

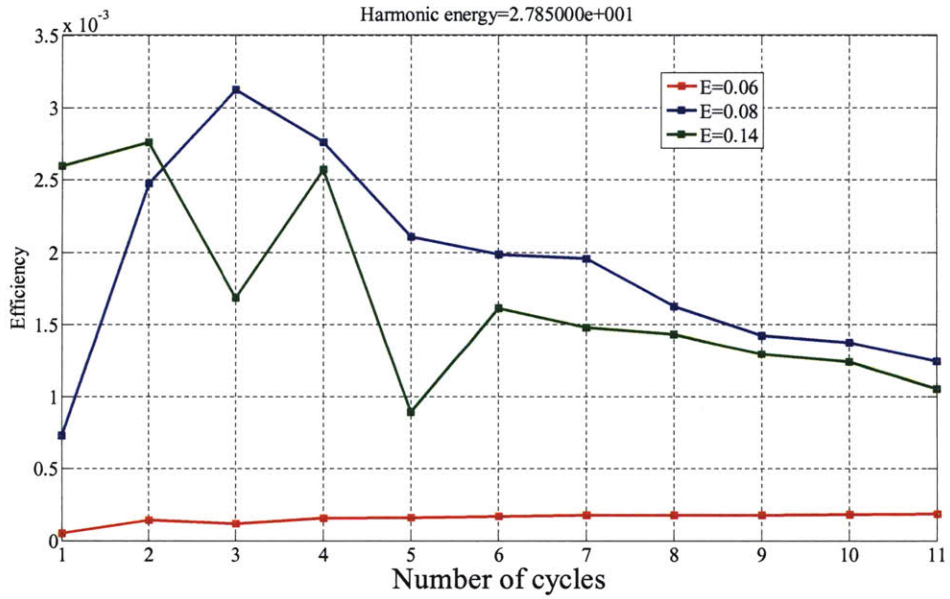

Figure 33: Harmonic efficiencies at Ninth Harmonic of 400nm driver pulse: 27.85 e.v.

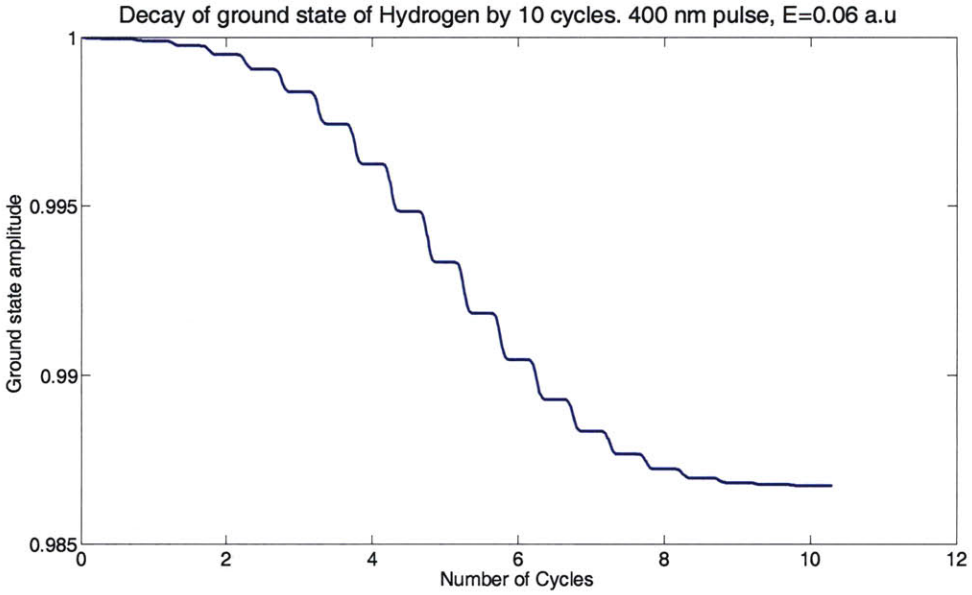

Figure 34: Ground state decay calculated by ADK formula for 400 nm,10 cycle pulse with E=0.06

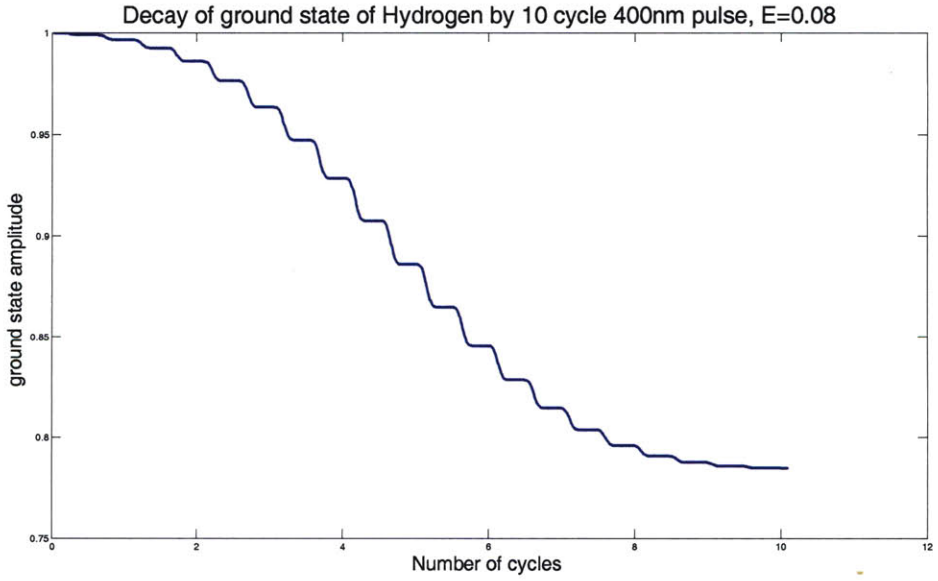

Figure 35: Ground state decay calculated by ADK formula for 400 nm,10 cycle pulse with E=0.08

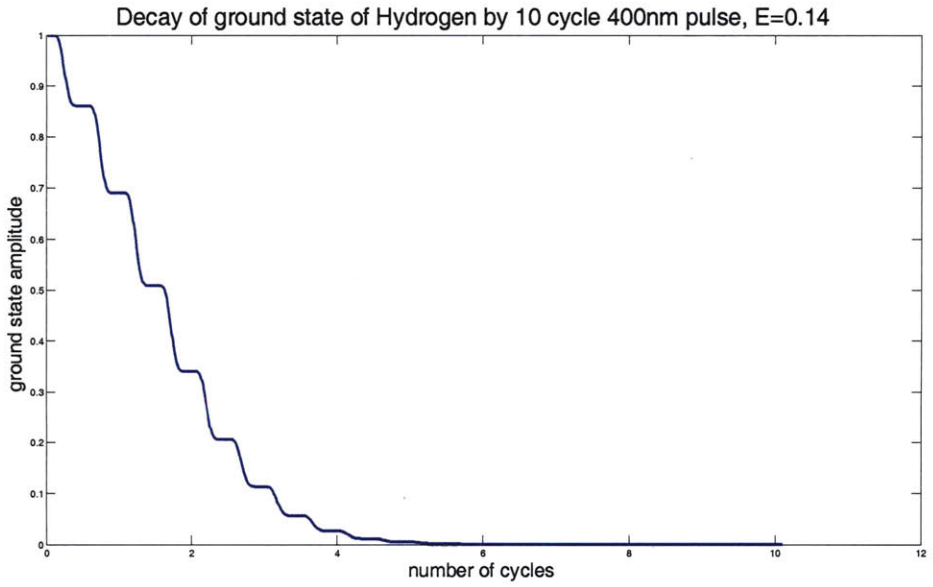

Figure 36: Ground state decay calculated by ADK formula for 400 nm,10 cycle pulse with E=0.14

3.4. Interaction of Hydrogen with 2000 nm pulse

Finally we look at $2000\,nm$ driver pulses for three different value of electric field. Due to longer wavelength, 2000 nm driver pulses have considerably larger cutoff than $400\,nm$ and $800\,nm$ pulses. Harmonic spectrum for three different cases of electric fields have been simulated as shown in the following table:

	Case 1	Case 2	Case 3
Electric Field (a.u.)	0.05	0.08	0.1
Cut-off (e.v.)	117.3	279.08	428.42
Keldysh Parameter	0.456	0.285	0.228

High Harmonic Spectrum of $10\,cycles$ driver pulse with $E = 0.05\,a.u.$, is shown in Figure 37. The odd harmonics are separated by $2\omega_0 = 1.24\,e.v.$ Figure 43, Figure 44 and Figure 45 show the ground state decay for $E = 0.05, E = 0.08$ and $E = 0.1$ respectively. For the same electric field strength and number of cycles, a driver pulse with longer wavelength causes more ground state depletion. For instance, for $E = 0.08$ and 10 cycles, a $400\,nm$ pulse ionizes about 20% of the ground state while a $2000\,nm$ pulse ionizes about 70% of the ground state.

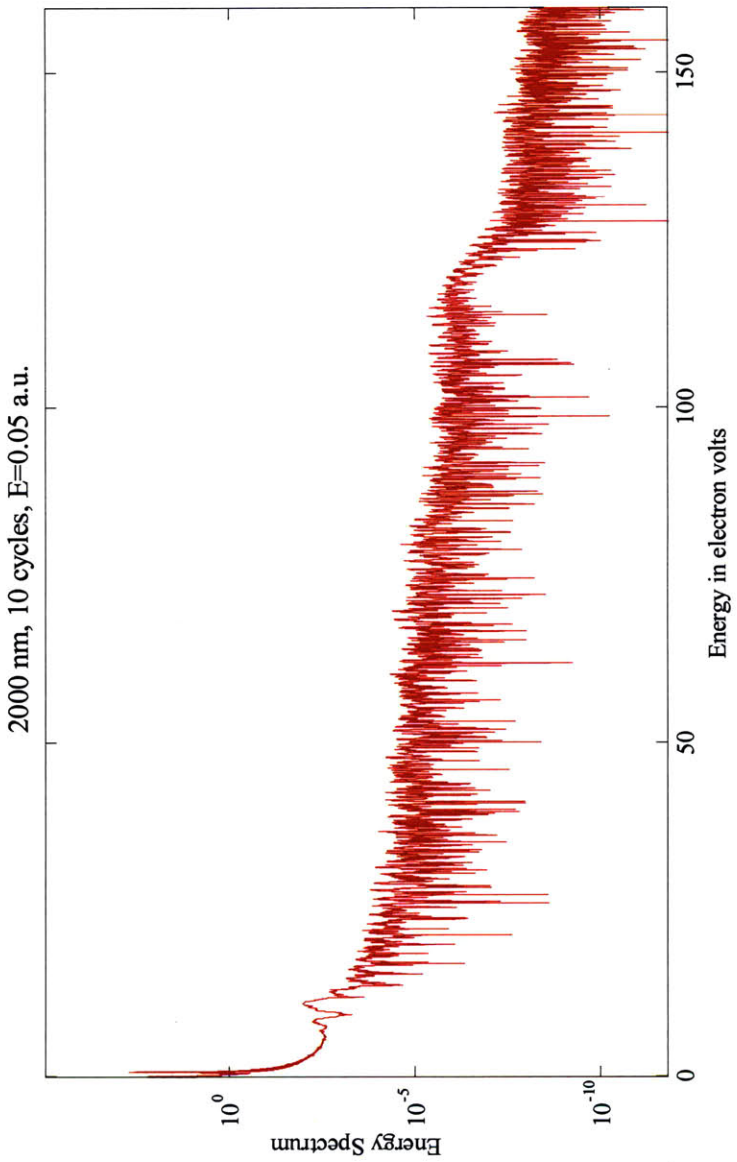

Figure 37: Energy spectrum of 2000nm driver pulse.

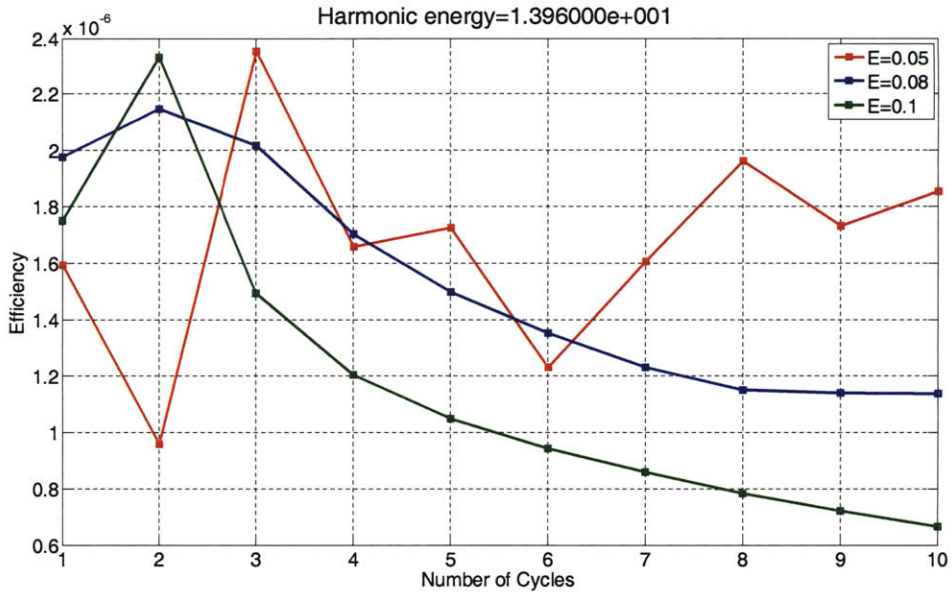

Figure 38 Harmonic efficiencies at 13.96 e.v. generated by 2000nm driver pulse.

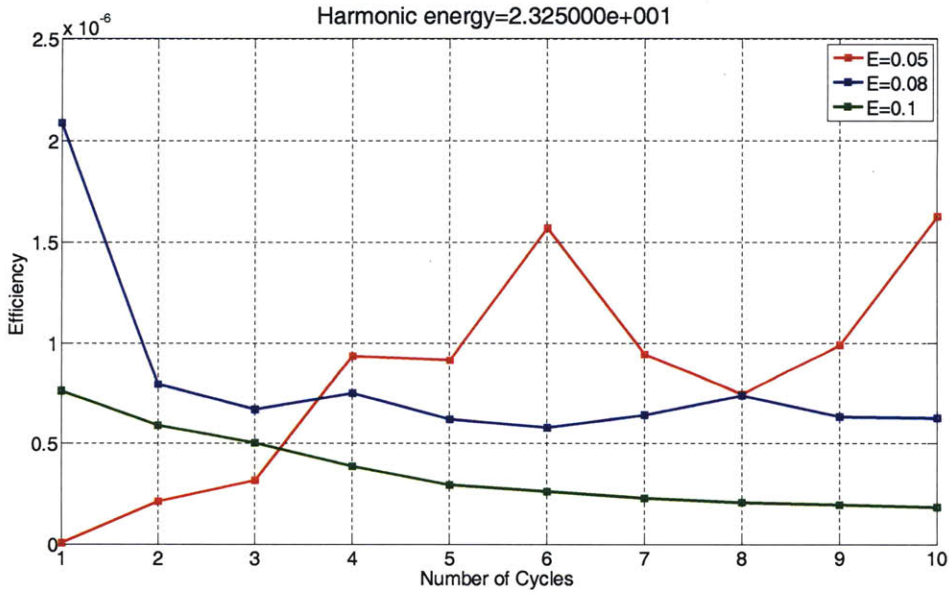

Figure 39 Harmonic efficiencies at 23.25 e.v. generated by 2000nm driver pulse.

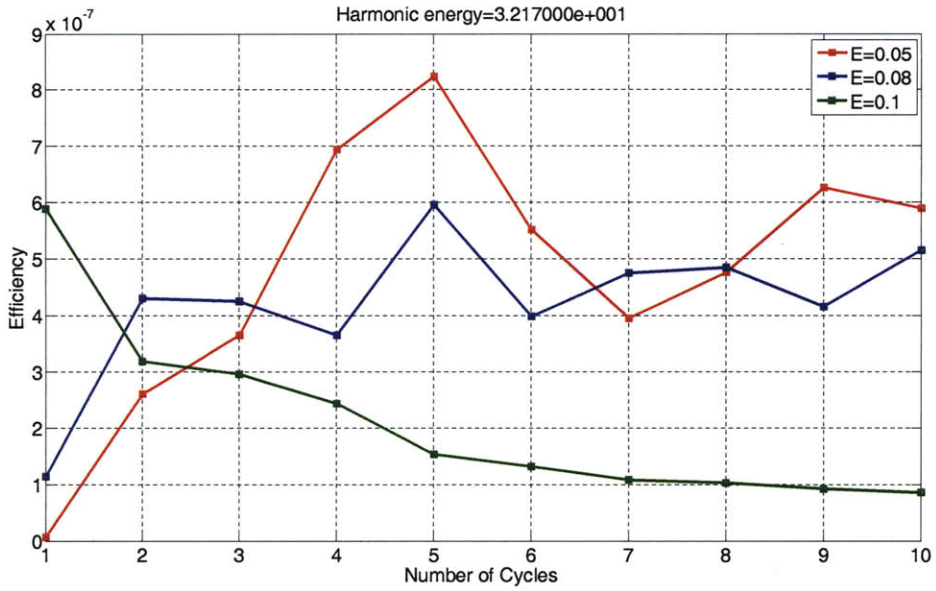

Figure 40: Harmonic efficiencies at 32.17 e.v. generated by 2000nm driver pulse.

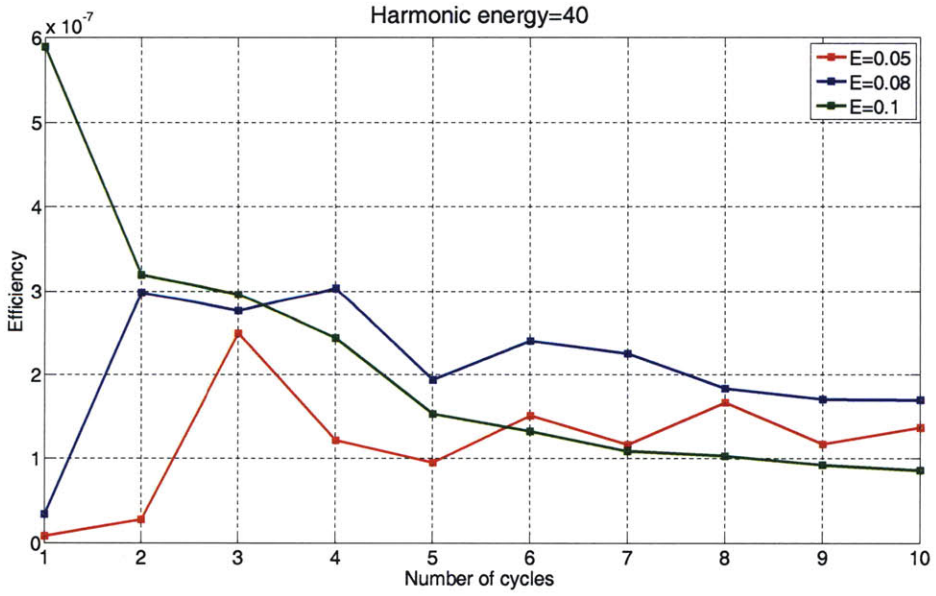

Figure 41 Harmonic efficiencies at 40 e.v. generated by 2000nm driver pulse.

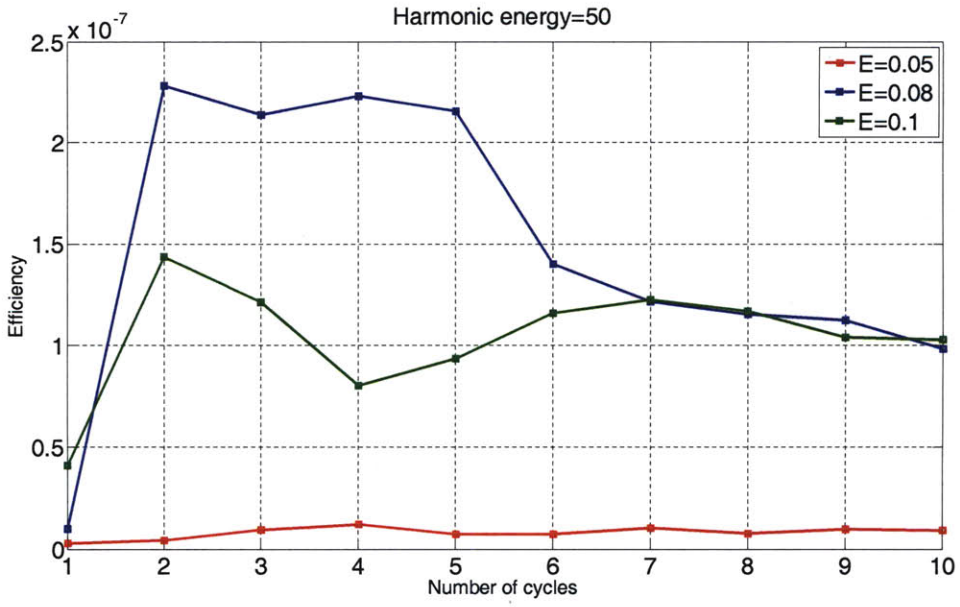

Figure 42: Harmonic efficiencies at 50 e.v. generated by 2000nm driver pulse.

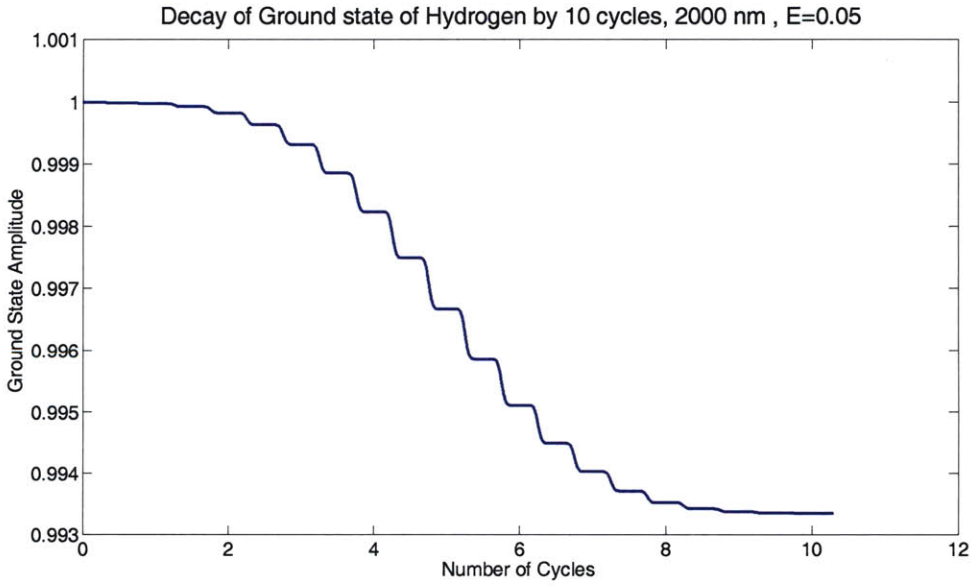

Figure 43: Ground state decay calculated by ADK formula for 400 nm,10 cycle pulse with E=0.14

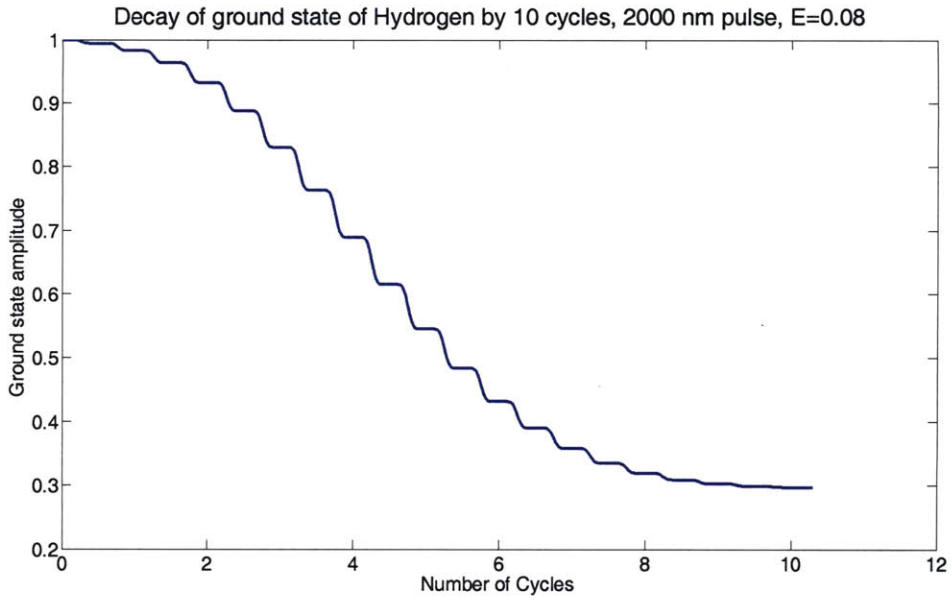

Figure 44: Ground state decay calculated by ADK formula for 400 nm,10 cycle pulse with E=0.14

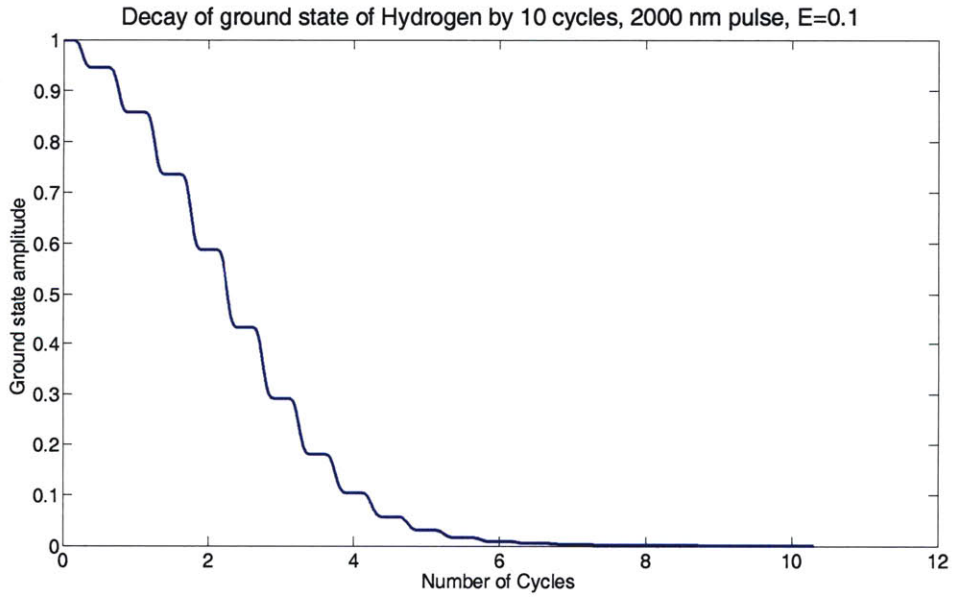

Figure 45: Ground state decay calculated by ADK formula for 400 nm,10 cycle pulse with E=0.14

3.5. Analysis

In the last three sections we saw the atomic efficiencies of different harmonic energies as a function of driver pulse duration and electric field. With this information, we will try to answer the question: in order to maximize the efficiency of a given harmonic energy, what is the ideal wavelength, pulse duration and electric field of the driver pulse?

First let us look at wavelength. From our data, shorter wavelengths have higher efficiencies. For example, at harmonic energy of $21 e.v.$, $400 nm$, $800 nm$ and $2000 nm$ driver pulses have efficiencies of $10^{-2}, 10^{-3}$ and 10^{-6} respectively. The time of return of electron of wave packet is linearly proportional to the driver wavelength (we will see more in this in Chapter 4.) Hence the electron wave packet undergoes larger quantum dispersion which reduces the recombination amplitude. As a result, the radiated harmonic energy decreases. Moreover, for a given electric field and number of cycles, a driver pulse with longer wavelength has more energy. Together, these two factors bring down the efficiency.

Next, we look at the role of electric field. If the electric field is too large, the atom will be completely ionized and harmonic radiation will be very small (see Figure 27.) If the electric field is too small then very little ionization will take place and HHG radiation will be small. It should be noted that ionization is exponentially dependent on electric field (see ADK formula. [5]) Only a small variation in the electric can lead large ionization difference. For instance, in Figure 25 we see that $E = 0.06$ (800 nm, 15 cycles) produce a small ionization of 4% If the electric field is doubled to $E = 0.12$, (800 nm, 15 cycles) as shown in Figure 27, almost the entire ground state is ionized. The optimum electric field depends on the position of the harmonic frequency in the spectrum (plateau or cut-off) and the number of cycles of the driver pulse. This is best illustrated in Figure 46 and Figure 47 which plot the efficiencies by an 800 nm driver pulse of duration of 4 cycles and 20 cycles respectively.

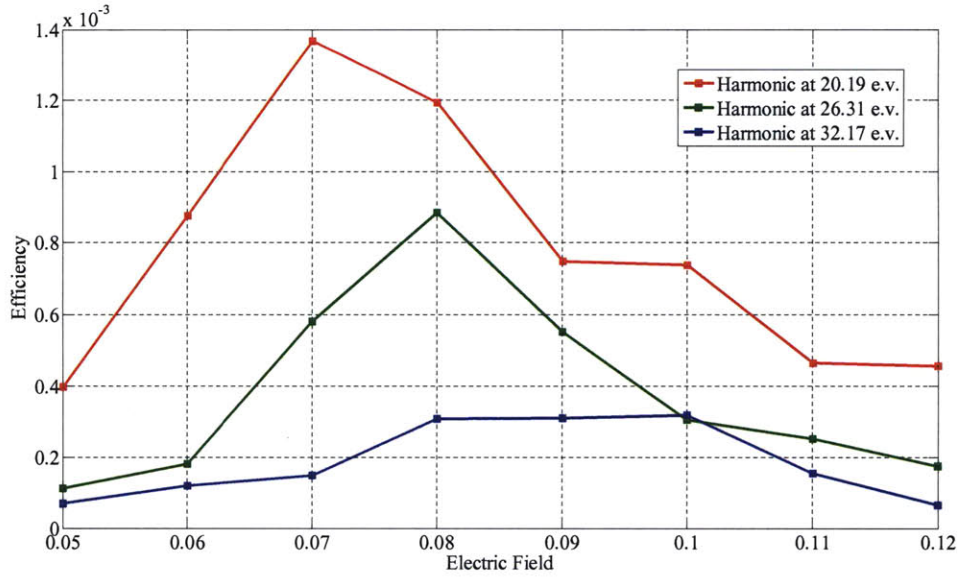

Figure 46: Efficiencies by a 4 cycle 800 nm driver pulse for different harmonic energies

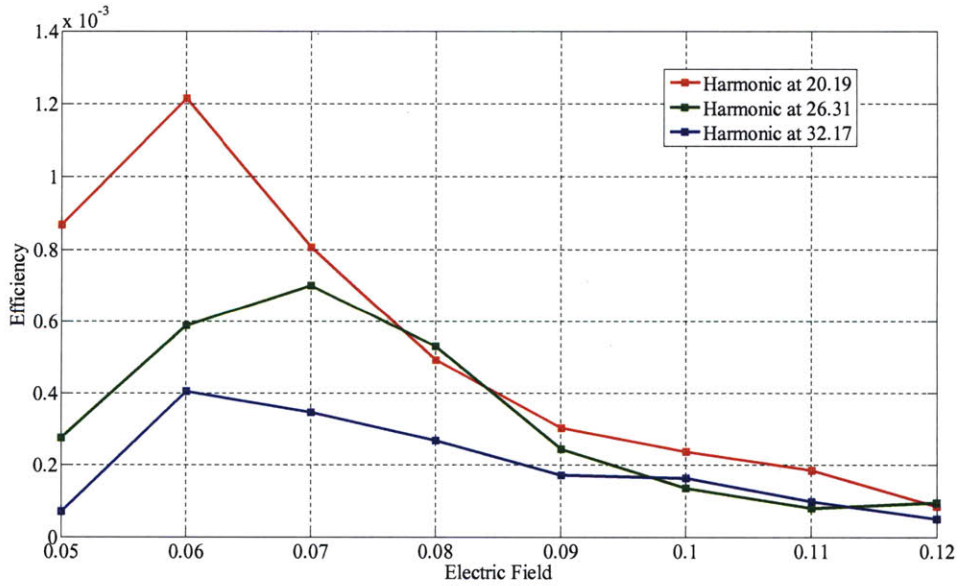

Figure 47: Efficiencies by a 20 cycle 800 nm driver pulse for different harmonic energies

Each harmonic has an optimum electric field which maximizes its efficiency. As we increase the number of cycles, the optimum electric field decreases. Moreover, this shift towards lower electric field is most dramatic for cut-off harmonic at $32.17 e.v.$: from $E = .11\ a.u$ for 4 cycles to $E = 0.06$ for 20 cycles. Additionally, the efficiency slightly increases from 3×10^{-4} to 4×10^{-4}. This shift in electric field is huge as dramatically changes the plasma density and is much better for phase matching. On the other hand, for plateau harmonic at $20.19 e.v.$, the shift is from $E = .07\ a.u$ to $E = .06$ and the efficiency decreases from 14×10^{-4} to 12×10^{-4}.

Since we are using a Gaussian pulse, contribution to the plateau harmonics comes from every cycle .But increasing the number of cycles also increases the total driver pulse energy and depletes the ground state. Together these factors bring down the efficiency of plateau-harmonics. On the other hand, harmonics in the cut-off region are produces only by the peak cycles. As the number of cycles increases, there are more cycles that contribute to cut-off harmonic. Therefore, as long as we use a small electric field, driver pulses with large number of cycles ($20-25 cycles$ for $E = 0.06$) produce higher efficiencies.

4. Gauge Transformation and the Role of Magnetic field

4.1. Gauge Transformation and High Harmonic Generation

In quantum mechanics, Schrödinger equation can be written in different equivalent gauges, because physical observables are gauge invariant. In HHG, Electron-Field interaction is mainly represented in two types of gauges, namely Goppert-Mayer gauge also known as the Length Gauge $(-e\mathbf{E}\cdot\mathbf{r})$ and Minimal coupling Hamiltonian also known as the Velocity gauge $\left(-\frac{e}{m}\mathbf{p}\cdot\mathbf{A}+\frac{e^2}{2m}\mathbf{A}^2\right)$. Since any physical problem is gauge invariant, we should be able to use either gauge to solve our Time Dependent Schrödinger Equation. Choice of gauge is not a new problem. Back in 1951, Lamb, in his seminal paper on Fine Structure of Hydrogen argued that theoretical calculation in Length Gauge was more convenient [17, 18]. Moreover, Strong field Approximation, which is often used in HHG theory, is not gauge invariant and is better suited for Length Gauge [19]. In this Chapter we will explore how the gauge transformations are done mathematically and what is the physical effect of such a transformation when coupled with dipole approximation.

4.2. Derivation of Gauge transformation.

According to the minimal coupling theory, Schrödinger of electron-electromagnetic field interaction is described as:

$$i\hbar\frac{\partial}{\partial t}\left|\Psi(t)\right\rangle=\left(\frac{(\mathbf{p}-q\mathbf{A}(\mathbf{r},t))^2}{2m}+qU(\mathbf{r},t)+V(\mathbf{r})\right)\left|\Psi(t)\right\rangle \tag{4.1}$$

In dipole approximation, $\mathbf{A}(\mathbf{r},t)\approx\mathbf{A}(t)$. The physical meaning of the approximation is that the wavelength of the EM field is longer than the length of interaction between electron and the field. Under this approximation (and using the atomic units $m=\hbar=e=1$), the Schrödinger equation becomes:

$$i\frac{\partial}{\partial t}\left|\Psi(t)\right\rangle_v = \left(\frac{(\mathbf{p}-\mathbf{A}(t))^2}{2} + U(\mathbf{r},t) + V(\mathbf{r})\right)\left|\Psi(t)\right\rangle_v \tag{4.2}$$

The v subscript denotes that this equation is written in Velocity Gauge. We can write this equation in Length Gauge through the following unitary transformation:

$$\left|\Psi\right\rangle_L = \hat{T}\left|\Psi\right\rangle_v \tag{4.3}$$

$$\hat{T} = e^{-i\mathbf{A}(t).\mathbf{r}} \tag{4.4}$$

Under such a gauge transformation, the Schrödinger equation changes in the following manner:

$$i\frac{\partial}{\partial t}\left|\Psi(t)\right\rangle_v = H_v\left|\Psi(t)\right\rangle_v \Rightarrow i\frac{\partial}{\partial t}\left|\Psi(t)\right\rangle_L = H_L\left|\Psi(t)\right\rangle_L \tag{4.5}$$

$$H_L = \hat{T}H_v\hat{T}^{\dagger} - i\hat{T}\frac{\partial \hat{T}^{\dagger}}{\partial t} \tag{4.6}$$

$$H_v = \frac{\mathbf{p}^2}{2} + \frac{\mathbf{A}(t)^2}{2} - \frac{\mathbf{p}.\mathbf{A}(t)}{2} - \frac{\mathbf{A}(t).\mathbf{p}}{2} + U(\mathbf{r},t) + V(\mathbf{r}) \tag{4.7}$$

$$= \frac{\mathbf{p}^2}{2} + \frac{\mathbf{A}(t)^2}{2} - \mathbf{A}(t).\mathbf{p} + V(\mathbf{r}) \tag{4.8}$$

In the above equation the following should be noted:

(i) $\mathbf{A}(t)$ and $\mathbf{p}$ commute because we are working in dipole approximation.

(ii) $U(\mathbf{r},t) = 0$, since we are working in coulomb gauge and charge distribution $\rho(\mathbf{r},t) = 0$.

Now using the transformation from (4.4) and projecting the Schrödinger equation in x-space

$$i\frac{\partial\Psi_L(\mathbf{r},t)}{\partial t} = \left[e^{-i\mathbf{A}(t).\mathbf{r}}\left(-\frac{\nabla^2}{2} + \frac{\mathbf{A}(t)^2}{2} + i\mathbf{A}(t).\nabla + V(\mathbf{r})\right)e^{i\mathbf{A}(t).\mathbf{r}} + \frac{\partial\mathbf{A}(t)}{\partial t}.\mathbf{r}\right]\Psi_L(\mathbf{r},t) \tag{4.9}$$

This transforms the Schrödinger equation to Length Gauge. Now, assume $\mathbf{A}(r) = A(r)\hat{z}$ and substitute it in (4.9). This implies that electric field is polarized in the z-direction. $\left(-\hat{\mathbf{z}}\frac{\partial A(t)}{\partial t} = \hat{\mathbf{z}}E(t)\right)$

$$-e^{-iA(t).r}\frac{\nabla^2}{2}e^{iA(t).r}\Psi(\mathbf{r},t)=\left[-\frac{\nabla^2}{2}-iA(t)\frac{\partial}{\partial z}+\frac{A(t)^2}{2}\right]\Psi(\mathbf{r},t) \tag{4.10}$$

$$e^{-iA(t).r}\mathbf{A}(t).\nabla e^{iA(t).r}\Psi(\mathbf{r},t)=\left[-A(t)^2+iA(t)\frac{\partial}{\partial z}\right]\Psi(\mathbf{r},t) \tag{4.11}$$

Substituting equation (4.10) and (4.11) in (4.9) finally gives us the Schroedinger Equation in dipole approximation.

$$\frac{\partial\Psi_L(\mathbf{r},t)}{\partial t}=\left[-\frac{\nabla^2}{2}+V(\mathbf{r})-E(t)z\right]\Psi_L(\mathbf{r},t) \tag{4.12}$$

The physical meaning of dipole approximation is that the trajectory of the ionized electron is much smaller than the wavelength of the driver field. Therefore, we can neglect the spatial dependence of the vector potential. A direct repercussion of this approximation is that we neglect the effect of magnetic field (which is present in a laser pulse.) The next step is to classically calculate the limits in which such an approximation is valid.

4.3. Role of Magnetic Field in HHG

The three step model assumes that after being born in the continuum, the electron only moves under the influence of the electric field. But in reality, Lorentz force due to the magnetic field also acts on it causing lateral displacement in the direction of propagation of the electric field. As a result, the electron may not "return back" to the atom. In quantum mechanical treatment we treat electron as a wavepacket. So the electron does not have to return exactly back to the electron for the recombination to occur. If quantum mechanical diffusion of the electron is less than the lateral displacement of the electron, recombination amplitude will drop.

Let us look at classical trajectory of the electron in a sinusoidal field assuming that it is born with zero velocity at the origin ($x(t=0)=0$). Like before, we are working in atomic units.

$$\ddot{x}(t)=F(t)=E_{0x}\cos(\omega t+\phi_B) \tag{4.13}$$

$$\dot{x}(t) = \frac{E_{0x}\sin(\omega t + \phi_B)}{\omega} + C_1 \tag{4.14}$$

$$x(t) = -\frac{E_{0x}\cos(\omega t + \phi_B)}{\omega^2} + C_1 t + C_2 \tag{4.15}$$

Where $C_1 = \frac{-E_{0x}\sin\phi_B}{\omega}$ and $C_2 = \frac{E_{0x}\cos(\phi_B)}{\omega^2}$.

$x(t)$: Position of electron trajectory.

ω : Angular frequency of driving field.

ϕ_B : Phase of birth of the electron.

E_{ox} : Electric field polarized along the x direction.

Lorentz Deviation

It is well known, form freshman physics, that when a charge moves in a magnetic field, a force acts on it, which is given by

$$\mathbf{F} = q(\mathbf{v} \times \mathbf{B}) \tag{4.16}$$

We can use this idea to calculate the deviation of the electronic wave packet

$$\ddot{z}(t) = F_z(t) \tag{4.17}$$

$$= \dot{x}(t)B_y(t) \tag{4.18}$$

$$= \left(\frac{E_{0x}\sin(\omega t + \phi_B)}{\omega} - \frac{E_{0x}\sin\phi_B}{\omega}\right)\frac{E_{0x}}{c}\cos(\omega t + \phi_B) \tag{4.19}$$

$$= \frac{E_{0x}^2\sin(2\omega t + 2\phi_B)}{2c\omega} - \frac{E_{0x}^2\cos(\omega t + \phi_B)\sin\phi_B}{c\omega} \tag{4.20}$$

Integrating the above equation and using the boundary condition that the velocity in y-direction at time of birth is zero gives

$$\dot{z}(t) = -\frac{E_{0x}^2\cos(2\omega t + 2\phi_B)}{4c\omega^2} - \frac{E_{0x}^2\sin(\omega t + \phi_B)\sin\phi_B}{c\omega^2} + C_3 \tag{4.21}$$

$$C_3 = \frac{E_{0x}^2\cos(2\phi_B)}{4c\omega^2} + \frac{E_{0x}^2\sin^2\phi_B}{c\omega^2} = \frac{E_{0x}^2}{4c\omega^2}(2 - \cos 2\phi_B) \tag{4.22}$$

Once again integrating equation and using the boundary condition that the position in y-direction at time of birth is zero gives

$$z(t) = -\frac{E_{0x}^2 \sin(2\omega t + 2\phi_B)}{8c\omega^3} + \frac{E_{0x}^2 \cos(\omega t + \phi_B)\sin\phi_B}{c\omega^3} + C_3 t + C_4 \tag{4.23}$$

$$C_4 = \frac{E_{0x}^2 \sin(2\phi_B)}{8c\omega^3} - \frac{E_{0x}^2 \sin 2\phi_B}{2c\omega^3} = -\frac{3E_{0x}^2 \sin(2\phi_B)}{8c\omega^3} \tag{4.24}$$

Quantum Diffusion

Now let us look at the quantum diffusion term. It is assumed that the when the electron is born, it is a Gaussian wavepacket (probability distribution perpendicular to the polarization) with FWHM of the dimensions of the Bohr radius (a_0) .The following derivation is taken from [20]

$$a_0 = 2\sqrt{2\ln 2}\sigma_0 \tag{4.25}$$

Momentum distribution is given by

$$\Phi(k) = \frac{A\sigma_0}{\sqrt{\pi}} \exp\left(-\sigma_0^2 (k - k_0)^2\right) \tag{4.26}$$

Corresponding wave function at zero time is

$$\Psi(x,0) = A\exp\left(-\frac{x^2}{4\sigma_0^2} + jk_0 x\right) \tag{4.27}$$

Taking the Fourier Transform of the wavefunction after the including the dispersion relation $\omega = \frac{k^2}{2}$ gives:

$$\Psi(x,t) = \frac{A\sigma_0}{\sqrt{\pi}} \int_{-\infty}^{\infty} dk \exp\left(-\sigma_0^2 (k - k_0)^2 - j\frac{k^2 t}{2} + jkx\right) \tag{4.28}$$

$$\Psi(x,t) = \frac{A}{\sqrt{1 + j\dfrac{t}{2\sigma_0^2}}} \exp\left(-\frac{x^2 - 4j\sigma_0^2 k_0 x + j2\sigma_0^2 k_0^2 t}{4\sigma_0^2\left(1 + j\dfrac{t}{2\sigma_0^2}\right)}\right) \tag{4.29}$$

And the corresponding probability distribution is:

$$|\Psi(x,t)|^2 = \frac{|A|^2}{\sqrt{1+\frac{t}{2\sigma_0^2}}} \exp\left(-\frac{(x-x_0(t))^2}{2\sigma_0^2\left(1+\left(\frac{t}{2\sigma_0^2}\right)^2\right)} \right) \tag{4.30}$$

$$x_0(t) = k_0 t \tag{4.31}$$

Now we have to incorporate the role of Lorentz force on the time evolution of the aforementioned probability distribution function. Firstly, note that k_0 corresponds to the mean of the momentum distribution. As a result, it should follow the classical trajectory under the influence of external force. Therefore, $k_0 \equiv k_0(t)$ and by classical relations $F(t) = \frac{dk_0(t)}{dt}$. As a result, the mean of the probability distribution moves classically (by Ehrnfest theorem) $x_0(t) = \int_0^t k_0(t')dt'$. This is the same as the lateral displacement by Lorentz displacement (given by $z(t)$). The new FWHM is given by:

$$a(t) = a_0\sqrt{1+\left(\frac{t}{2\sigma_0^2}\right)^2} \tag{4.32}$$

In the following figures (Figure 48 to Figure 50) we plot the HWHM $\left(\frac{a(t)}{2}\right)$ at the probability distribution of the wave packet at the time of return. The phase of birth is assumed to be $\frac{\pi}{8}$ (which corresponds to the most energetic trajectory).

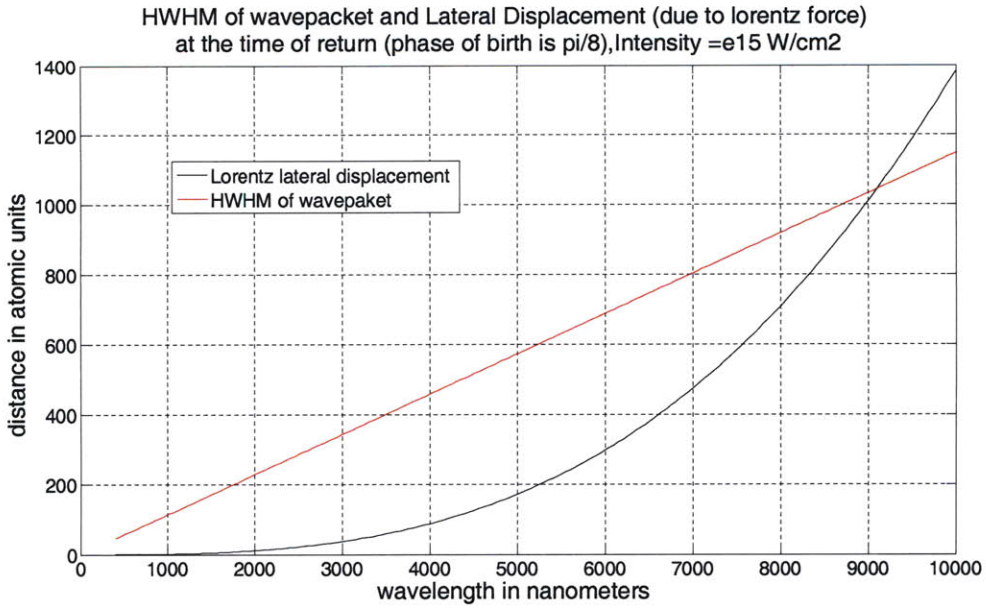

Figure 48 Comparison of Lorentz displacement and quantum diffusion

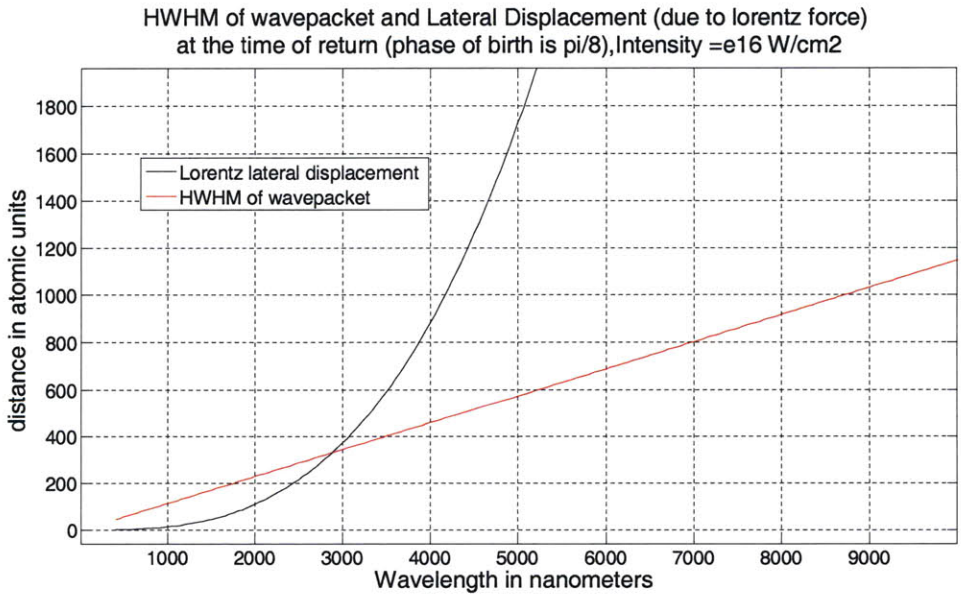

Figure 49 Comparison of Lorentz displacement and quantum diffusion

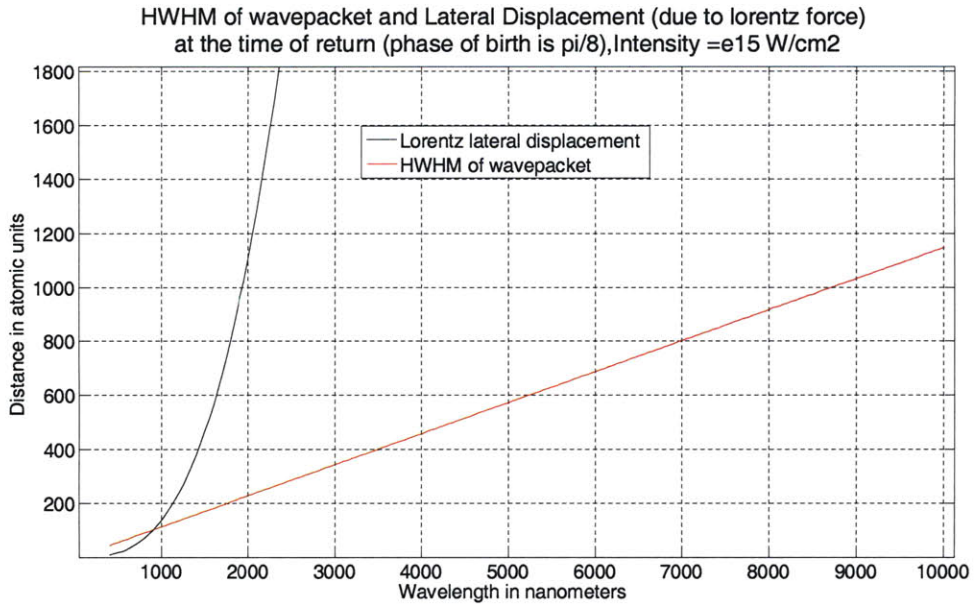

Figure 50 Comparison of Lorentz displacement and quantum diffusion

Few things to note in the above plots are:

(i) If the electron was classical point particle, there would be no recombination event due to Lorentz displacement. Treating it as a wavepacket, gives a non-zero recombination probability even when it is displaced from the axis of polarization: provided the broadening of the wavepacket, due to quantum dispersion, is more than the lateral displacement.

(ii) Quantum dispersion (hence the time of return) scales linearly with wavelength while the Lorentz displacement term scales as cube of wavelength.

(iii) Quantum dispersion (hence the time of return) does not depend on intensity where as the Lorentz displacement term scales linearly with intensity.

Since people are pushing for longer wavelength driving fields [21], it becomes all the more important that we consider the role of magnetic field. One of the ideas, which we tested to reduce the Lorentz displacement was to use an elliptically polarized light. The two polarizations of the elliptically polarized light can be phase shifted to cancel out the Lorentz displacement. However, in this case it is the electric field that becomes the problem. Not only does it displace the wavepacket from the atom, fewer trajectories return back as the phase difference between the two polarization increases.

In the following figures we look at the dependence of electron trajectory on the ellipticity of polarization Electrons which are born in red portion of the electric field, return back to the atom. Here "eturning back" is loosely defined: it refers to those electrons whose distance from the atom increases up to a time instant, and after which it begins to decrease.

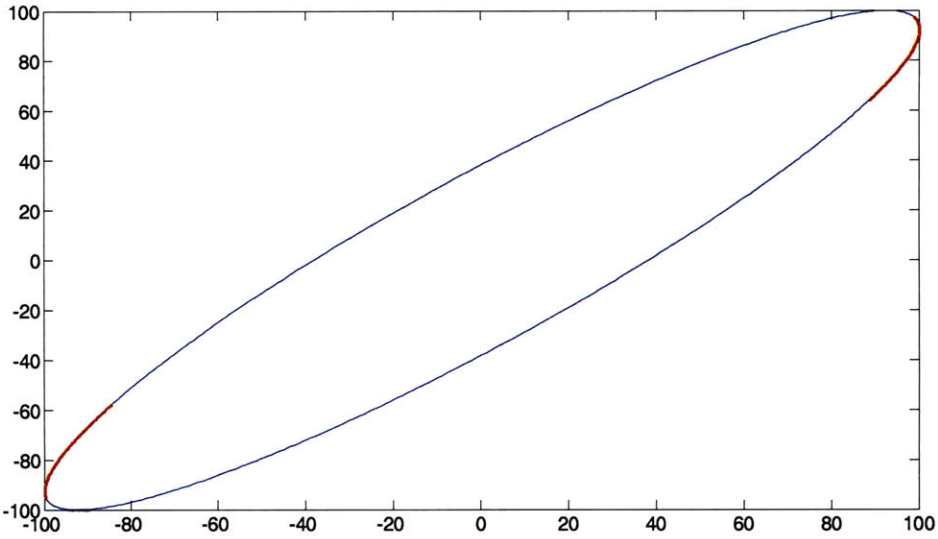

Figure 51 Trajectories that are born in the highlighted part of the electric field return back to the atom. Polarization rotates clockwise (temporally.) Phase difference between x and y polarization is pi/8

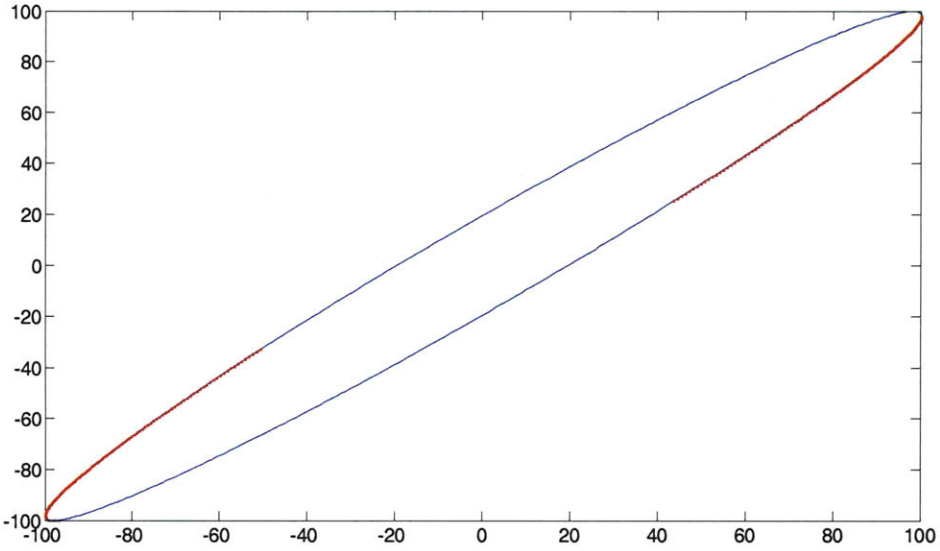

Figure 52 Trajectories that are born in the highlighted part of the electric field return back to the atom. Polarization rotates clockwise (temporally.) Phase difference between x and y polarization is pi/16.

4.4. Conclusion

In this chapter the mathematical foundation of gauge transformation was re-derived. Hamiltonian of atom-field interaction was transformed from velocity gauge to length gauge (provided we work in Coulomb Gauge $(\nabla \bullet A = 0)$ and assume Dipole Approximation $(\mathbf{A}(\mathbf{r},t) = A(t))$). Due to Dipole Approximation magnetic field is forced to be zero. Magnetic field, which leads to lateral Lorentz displacement, was incorporated classically. It was then quantitatively argued that if the Lorentz displacement is more than the Half Width Half Maximum (HWHM) of the returning wave packet probability distribution, the recombination amplitude should drop considerably. The HWHM is independent of the driving field intensity and increases linearly with wavelength. Lorentz displacement, on the other hand, varies linearly with driving intensity and cubic with driving wavelength. Therefore, for long wavelengths and large intensities, Lorentz displacement becomes large and recombination amplitude decreases

Lorentz displacement can be reduced using circularly polarized light because the magnetic fields of the two polarizations cancel each other out. But the electric field prevents

the electronic wave packet from returning. Another way of reducing the Lorentz displacement is to use counter propagating wave such that the electric field points in the same direction but magnetic fields cancel each other out.

5. References

1. Brabec, T. and F. Krausz, *Intense few-cycle laser fields: Frontiers of nonlinear optics.* Reviews of Modern Physics, 2000. **72**(2): p. 545-91.
2. Agostini, P. and L.F. DiMauro, *The physics of attosecond light pulses (vol 67, pg 813, 2004).* Reports on Progress in Physics, 2004. **67**(8): p. 1563-1563.
3. Corkum, P.B. and F. Krausz, *Attosecond science.* Nature Physics, 2007. **3**(6): p. 381-387.
4. Ammosov, M.V., et al., *Tunneling Ionization of Atoms and Atomic Ions in an Intense Laser Field with a Nonhomogeneous Space-Time Distribution.* Journal of the Optical Society of America B-Optical Physics, 1992. **9**(8): p. 1225-1230.
5. Ammosov, M.V., N.B. Delone, and V.P. Krainov, *Tunnel Ionization of Complex Atoms and Atomic Ions in a Varying Electromagnetic-Field.* Zhurnal Eksperimentalnoi I Teoreticheskoi Fiziki, 1986. **91**(6): p. 2008-2013.
6. Gordon, A. and F. Kaertner, *High Harmonic Generation Research Notes.*
7. Ivanov, M.Y., M. Spanner, and O. Smirnova, *Anatomy of strong field ionization.* J. Mod. Opt., 2005. **52**(2-3): p. 165-184.
8. Gordon, A. and F.X. Kärtner, *Quantitative modeling of single atom high harmonic generation.* Phys. Rev. Lett., 2005. **95**: p. 223901-1-4.
9. Gordon, A. and F.X. Kartner, *First-order strong field approximation for high-order harmonic generation.* 2006.
10. Protopapas, M., et al., *Recollisions, bremsstrahlung, and attosecond pulses from intense laser fields.* Physical Review A, 1996. **53**(5): p. R2933-R2936.
11. Gordon, A., C. Jirauschek, and F.X. Kartner, *Numerical solver of the time-dependent Schrodinger equation with Coulomb singularities.* Physical Review A, 2006. **73**(4): p. -.
12. Christov, I.P., M.M. Murnane, and H.C. Kapteyn, *High-Harmonic Generation of Attosecond Pulses in the "Single-Cycle" Regime.* Phys. Rev. Lett., 1997. **78**(7): p. 1251-1254.
13. Hu, S.X. and L.A. Collins, *Intense laser-induced recombination: The inverse above-threshold ionization process.* Physical Review A, 2004. **70**(1): p. 013407.
14. Gordon, A., R. Santra, and F.X. Kärtner, *Role of the Coulomb singularity in high harmonic generation.* Phys. Rev. A, 2005. **72**: p. 063411-1-7.
15. Ivanov, M.Y., T. Brabec, and N. Burnett, *Coulomb corrections and polarization effects in high-intensity high-harmonic emission.* Physical Review A, 1996. **54**(1): p. 742.
16. Lehtovaara, L., J. Toivanen, and J. Eloranta, *Solution of time-independent Schrodinger equation by the imaginary time propagation method.* Journal of Computational Physics, 2007. **221**(1): p. 148-157.
17. Lamb, W.E., *Fine Structure of the Hydrogen Atom .3.* Physical Review, 1952. **85**(2): p. 259-276.
18. Lamb, W.E., R.R. Schlicher, and M.O. Scully, *Matter-Field Interaction in Atomic Physics and Quantum Optics.* Physical Review A, 1987. **36**(6): p. 2763-2772.

19. Chen, J. and S.G. Chen, *Gauge problem in molecular high-order harmonic generation.* Physical Review A, 2007. **75**(4): p. -.
20. Kaertner, F., *Fundamental of Photonics Lecture Notes.*
21. Gordon, A. and F.X. Kärtner, *Scaling of keV HHG photon yield with drive wavelength.* Opt. Expr., 2005. **13**: p. 2941-2947.